Check for updates

The paleotectonic evolution of the western Mediterranean: provenance insights from the internal Betics, southern Spain

Eirini M. Poulaki* and Daniel F. Stockli

Department of Geosciences, The University of Texas at Austin, Austin, TX, United States

Since the early Cenozoic, the closure of the Alpine Tethys in the Western Mediterranean has been accomplished by protracted subduction, followed by collision and orogenic collapse. The internal zones of the Betic Cordillera (southern Spain) and Rif (northern Morocco) experienced subduction metamorphism and subsequent exhumation due to the westward migration of the orogenic system. The detrital provenance of these meta-sedimentary units contains crucial insights into their pre-subduction stratigraphic arrangement, which is essential to constrain the pre-Cenozoic paleogeography and tectonic evolution of the Western Mediterranean. This study focuses on the Nevado-Filábride Complex (NFC) and the Eastern Alpujárride Complex in the Internal Betic Cordillera. New depth-profile zircon U-Pb LA-ICP-MS data from the NFC (N = 72) and Alpujárride (N = 21) and *in situ* apatite U-Pb data from a metabasite within the NFC allow us to establish the pre-subduction stratigraphy, sedimentary provenance, and paleotectonic configuration of the Iberian rifted margin during the Paleozoic−Early Mesozoic. Our dataset demonstrates that the NFC represents an intact Devonian to Early Jurassic stratigraphic sequence that records the evolution of the Western Mediterranean from the Variscan orogeny to rifting and opening of the Alpine Tethys. Detrital zircon U-Pb age modes of the NFC remain remarkably similar for over 200 Myr with only the differences being the progressive addition of new zircon modes related to depositional ages. Additionally, a comparison between the provenance record of the NFC and Alpujárride reveals notably similar zircon signatures of Carboniferous and Permian strata. This study reports the first data from the Triassic−Jurassic strata that record the opening of the Alpine Tethys. Additional evidence for rifting is present in the metabasites from the Veleta unit yielding *in situ* apatite U-Pb ages of 197 Ma, recording CAMP magmatism and Early Jurassic rifting in the Alpine Tethys. The data demonstrate a palinspastic connection between the NFC and the Alpujárride. Based on these extensive new provenance data, we propose a pre-subduction tectonic configuration in which the NFC and Alpujárride both represent adjacent attenuated continental fragments that are separated from the southern Iberian rifted margin by a narrow oceanic domain of the Alpine Tethys in the early Mesozoic.

1 Introduction

Subduction complexes expose rocks that have been subducted to great depths and subsequently exhumed back to the surface. These complexes are typically investigated to elucidate tectono-metamorphic processes of subduction zones, yet these highly deformed and metamorphosed rocks also record a rich record of their pre-subduction histories, such as paleogeography and stratigraphy. In particular, the Detrital Zircon (DZ) provenance record has the potential to unlock this information from these geologic units and provide critical insights into the paleogeography, tectonic affinity, and pre-subduction stratigraphic evolution—thus providing powerful constraints on plate tectonics' reconstructions. The Mediterranean region is particularly well-suited to this avenue of study as it exposes several exhumed subduction complexes that record oceanic and continental subduction in response to the closure of the Neotethys from the Aegean, the Alps, to the Betics. The complicated tectonic history of the Mediterranean is mainly attributable to the presence of a number of distinct oceanic and rifted continental domains which were either subducted and/or accreted in relatively short subduction–collision cycles (Royden & Faccenna, 2018). In the Mediterranean, subduction zones were generally short-lived and involved subduction and accretion of segmented oceanic and/or exhumed mantle lithosphere domains and rifted/hyperextended continental margins rifted off the Tethyan continental margin during the protracted and spatially complex opening and closure of the Neotethys. This segmented tectonic architecture has been a hallmark of Mediterranean tectonics and continues to the present. The rapidity and spatial heterogeneity of this tectonic evolution have made it challenging to reconstruct the geologic history of the Mediterranean using traditional structural and stratigraphic methods alone.

Plate reconstructions of the Western Mediterranean appear to have been largely controlled by the kinematic framework of the Atlantic and Alpine Tethys (Sibuet et al., 2004; Vissers and Meijer, 2012; Barnett-Moore et al., 2016; Nirrengarten et al., 2018). Major tectonic events from the early Mesozoic to the late Cenozoic, such as the breakup of Pangea, Alpine collision, and Cenozoic rollback have resulted in a large number of isolated tectonic continental fragments. When the main plate motions and convergence rates generally agree among various studies, the tectonic evolution of specific terranes or the paleogeographic positions, in particular subducted and underplated terranes, often remain enigmatic and debated. Conceptual models highlight significant disparities in the number of oceanic domains, the position of fragmented microplates, and the polarity and number of subduction zones during the Cenozoic within the Western Mediterranean (Van Hinsbergen et al., 2020; Guerrera et al., 2021).

This study focuses on one of the most extensive, yet poorly understood, subduction complexes in the Western Mediterranean, the Nevado-Filábride Complex (NFC), and Eastern Alpujárride of the Betic Cordillera in southern Spain (Figure 1). The Betic Cordillera is a narrow mountain range that formed during convergence between Africa and Eurasia in the Cenozoic (Dewey et al., 1989; Zeck, 1996; Lonergan & White, 1997; Carminati et al., 1998; Faccenna et al., 2004; Platt, 2007). The Betic Cordillera has been divided into Internal and External zones reflecting their tectonic position within the collision orogen–with the Internal Betic terranes closer to the orogenic core, while the External Betics are thrust over the Guadalquivir foreland basin. The Internal Betics are subcategorized, structurally from top to bottom, into the Maláguide, Alpujárride, and NFC, of which the NFC represents the structurally lowest unit that underwent penetrative deformation and high-pressure/low-temperature (HP/LT) metamorphism during subduction and subsequent exhumation. The Internal Betics have been considered to represent part of the original Alboran domain (Balanyá et al., 1987), an allochthonous and highly attenuated block that now underlies the Alboran Sea between the Betic Cordillera in southern Spain and the conjugate Rif Cordillera in northern Morocco. However, several recent studies have correlated the NFC tectonically to the southern Iberian rifted margin (Booth-Rea et al., 2007; Behr & Platt, 2012; Gómez-Pugnaire et al., 2012; Platt et al., 2013; Rodriguez-Cañero et al., 2018). The complex metamorphic and deformation history that the rocks experienced during the Variscan and Alpine orogenies from the NFC and Alpujárride have hampered our understanding of their provenance, internal stratigraphy, and paleogeographic position in relation to the Iberian and African continental margins.

In this study, we leveraged systematic and extensive new sedimentary provenance data to reconstruct the tectonostratigraphic evolution of the NFC and its spatial relationship with the Eastern part of the Alpujárride Complex, both of which now lie within the Internal Betic Cordillera of southern Spain (Figure 1). These new detrital and magmatic zircon U-Pb and *in situ* apatite U-Pb analyses from one metabasite, combined with petrographic field observations allow us to illuminate the Paleozoic–Mesozoic provenance history, the pre-subduction stratigraphy, and paleotectonic affinity and evolution of the NFC and Alpujárride complex. We used these new constraints to evaluate the relationship
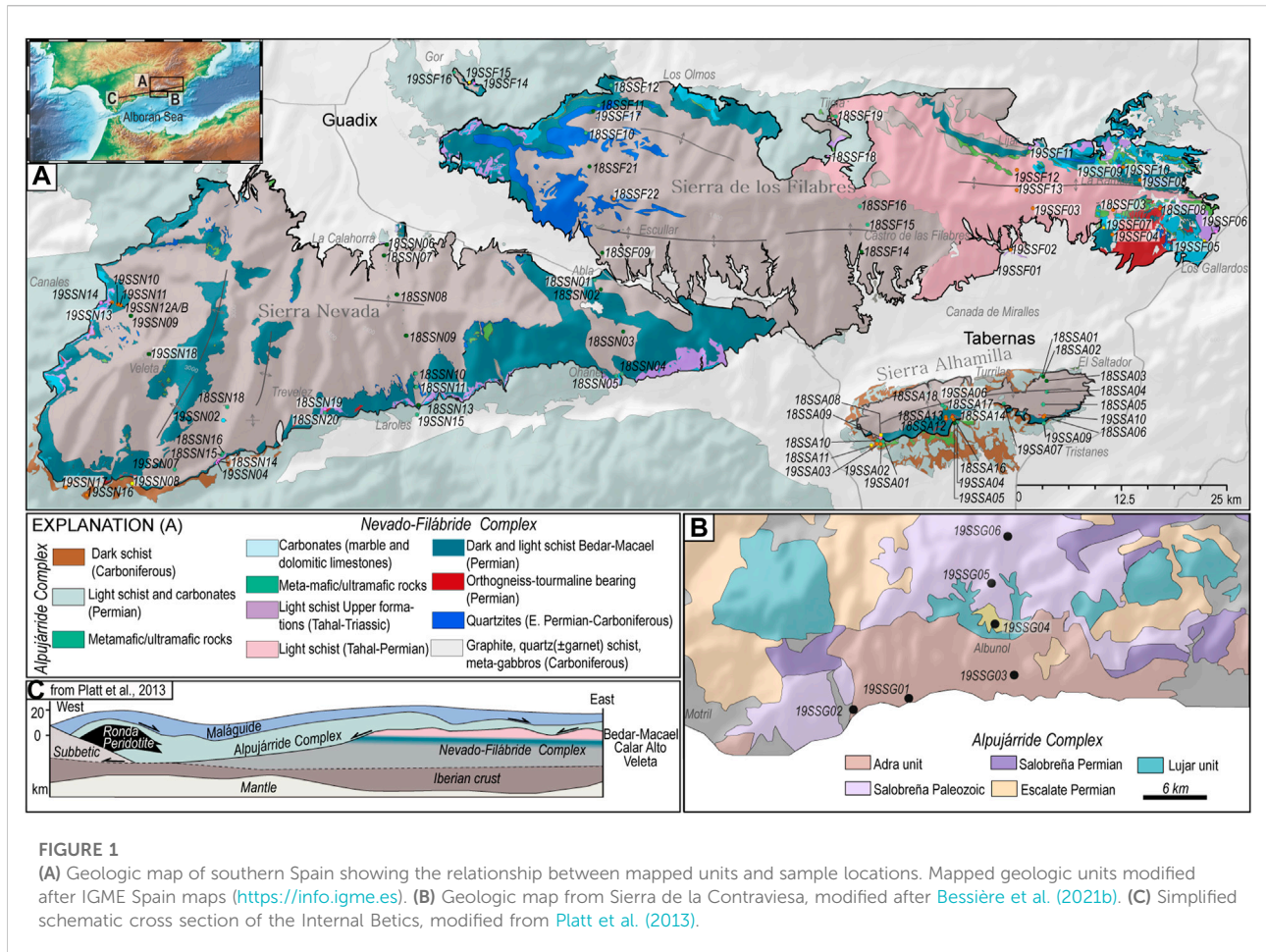
FIGURE 1
(A) Geologic map of southern Spain showing the relationship between mapped units and sample locations. Mapped geologic units modified after IGME Spain maps (https://info.igme.es). **(B)** Geologic map from Sierra de la Contraviesa, modified after Bessière et al. (2021b). **(C)** Simplified schematic cross section of the Internal Betics, modified from Platt et al. (2013).

between the NFC and Alpujárride, their affinity with respect to the Iberian margin, and the implications for the tectonic evolution of the Alpine Tethys in the Mediterranean realm from the Paleozoic to Mesozoic.

2 Geologic setting

2.1 Evolution of the Western Mediterranean

The Western Mediterranean has experienced rapidly evolving tectonic cycles since the Paleozoic, involving numerous abrupt switches between extensional and contractional events (Gomez et al., 2019). The Variscan orogeny was a widespread continental collision in the Late Paleozoic as part of the final amalgamation of Pangea. The record of orogenesis dominated the basement geology throughout western and southwestern Europe and is characterized by several roughly E–W trending tectonic belts composed of Avalonia, Armorican, and Gondwanan autochthonous and allochthonous sedimentary, magmatic, and metamorphic terranes (Leprêtre et al., 2018). During this time, Iberia, shows a very strong Proterozoic NE African Algerian (Schettino & Turco, 2009; Handy et al., 2010; Sibuet et al., 2012; Biari et al., 2017; Nirrengarten et al., 2018) Postorogenic magmatism during the Late Carboniferous–Early Permian, marked the transition from collision to orogenic collapse and widespread extension in the internal Variscan domain (de Saint Blanquat et al., 1990; Vissers, 1992; de Saint Blanquat, 1993; Saspiturry et al., 2019). During the early Mesozoic, the Mediterranean experienced the closure of the Paleo-Tethys and the subsequent opening of the Neotethys in the eastern Mediterranean realm, while in the west, rifting associated with the opening of the central Atlantic led to continental break-up and opening of the Alpine Tethys in the Jurassic. Jurassic rifting was complex and resulted in hyperextended crustal and exhumed mantle domains and the creation of numerous distended continental fragments and ribbons (e.g., Mohn et al., 2010). This tectonic evolution of the Tethys resulted in complex paleogeography composed of ribbon continents, attenuated crust, segmented continental basin systems, and small oceanic

and hyperextended basins (Dercourt et al., 1986; Stampfli & Borel, 2002; Csontos & Vörös, 2004; Gaina et al., 2013). Geologic evidence supports the existence of isolated rifted continental fragments of Eurasian, Iberian, and African (Gondwanan) affinities with intervening oceanic basins and significant structural and stratigraphic heterogeneity, although the relative position and fate of these blocks remain debated because the proposed oceans separating them have mostly disappeared and been consumed by late Mesozoic and Cenozoic subduction (Dercourt et al., 1986).

The precise paleogeography of the continental and oceanic domains in the Alpine Tethys during the Jurassic remains elusive and debated due to the complicated tectonic evolution during early Mesozoic rifting and Cenozoic subduction and exhumation. Controversies have arisen over the number and nature of oceanic domains during this period with studies proposing scenarios ranging from a single to multiple segmented oceanic regions (e.g., Ligurian Tethys, Betic ocean, and Maghrebian Tethys). The Ligurian or Alpine Tethys is a proposed western domain that linked the Neotethys and the central Atlantic and opened between 185 and 150 Ma (e.g., Manatschal & Müntener, 2009; Puga et al., 2011). The opening of the Alpine Tethys resulted in the separation of the AlKaPeCa (Alboran–Kabylian–Peloritan–Calabrian) continental block from the southwestern margin of Europe. The paleogeographic position of AlKaPeCa has been thought to be the result of this separation from southwestern Europe (Bouillin et al., 1986) but either remained as part of the Iberian margin (e.g., Chalouan et al., 2008) or became adrift within the Alpine Tethys (e.g., Guerrera et al., 2012). The exact paleogeographic position of the AlKaPeCa block is poorly constrained as it may have experienced hundreds of kilometers of tectonic translation from its original position. In addition, the individual terranes that originally constituted the AlKaPeCa block are now scattered throughout the western Mediterranean region (van Hinsbergen et al., 2014; Leprêtre et al., 2018; Romagny et al., 2020; van Hinsbergen et al., 2020). An alternative scenario suggests the existence of a Mesomediterranean microplate, a continental block that rifted from Pangea and resided between Africa and Eurasia, straddled by two major arms of the Tethyan oceanic domains (Guerrera et al., 1993, 2005).

In the Late Cretaceous, the opening of the Equatorial Atlantic triggered northward translation and counter-clockwise rotation of Africa and resulted in convergence and collision between Africa and Eurasia. Much of the intermediate oceanic, exhumed mantle, or highly attenuated continental crust were subducted, and the continental blocks were highly deformed and metamorphosed during the Cenozoic collision, hindering our understanding of Western Mediterranean architecture before this period. Ongoing convergence between Africa and Iberia sparked subduction initiation in the Western Mediterranean. The position, polarity, nature, and timing of subduction in the late Mesozoic and Cenozoic are highly debated. One scenario

involves a single subduction zone along southern Iberia (Sainz and Faccenna, 2001) with geophysical and geodynamic studies supporting a north-dipping subduction zone starting at least in the Miocene (Zeck, 1996; Lonergan & White, 1997; Calvert et al., 2000; Brun & Faccenna, 2008; Lis Mancilla et al., 2013; van Hinsbergen et al., 2014; Williams & Platt, 2018). Geological evidence also corroborates a north-northwest dipping subduction scenario (Rosenbaum et al., 2002; Faccenna et al., 2004; Booth-Rea et al., 2007; Bezada et al., 2013; Chertova et al., 2014). Alternatively, several studies have proposed that subduction may have first begun with a south-dipping slab, followed by polarity reversal to northwest-dipping subduction (Rehault et al., 1984; Frizon de Lamotte et al., 2000; Carminati et al., 2012; Behr & Platt, 2013). A third prominent hypothesis invokes a doubly vergent subduction system with two simultaneous slabs sinking toward the NW and SE (Vergés & Fernàndez, 2012; Bessière et al., 2021a).

Since the late Miocene, rapid slab rollback has caused widespread extension in the overriding plate, resulting in the separation and translation of crustal blocks (e.g., Corsica and Sardinia) and the formation of new oceanic crust between Spain and Italy, while the trench swept to its present-day position in the Gibraltar Arc to the west of the Alboran Sea. This tectonic rearrangement also separated the Alboran domain from the AlKaPeCa block and translated it to the Alboran Sea and Betic-Rif Cordilleras. The switch to extension resulted in core complex formation and thinning of continental crust beneath the Alboran Sea and continues today as evidenced by seismicity and active faulting (Gonzalez-Castillo et al., 2015; Grevemeyer et al., 2015). The current arrangement of the Betic–Rif Cordillera and Gibraltar subduction zone is unique in that it forms one of the tightest mountain belts on Earth and is linked to rollback and translation since the Late Miocene.

The External domain of the Betic Cordillera comprises thrust sheets of Mesozoic and Cenozoic strata, deposited along the Iberian continental margin, and thrust over Miocene sedimentary rocks of the Guadalquivir foreland basin. The Internal Betics are thought to represent stacks of various continental terranes that were thrust onto the Iberian plate. The Maláguide and Alpujárride terranes have equivalents in the Rif Cordillera of Morocco based on similar petrographic and metamorphic characteristics and correlated as Maláguide-Ghomaride and Alpujárride-Sebtite (Balanyá et al., 1987). Interestingly, the NFC does not appear to have an apparent Rif-equivalent, which led some studies to suggest the NFC origins are not linked to Alpujárride and Maláguide. Nevertheless, the similarities between the Betic and Rif zones are linked through Cenozoic subduction and Miocene collision of the Alboran domain with the southern Iberian and Northern Maghrebian margins. More recent studies have challenged the notion of linking the NFC to the allochthonous Alboran domain; instead, proposing these units were always proximal to the southern margin of the Iberian Peninsula (e.g., Gómez-
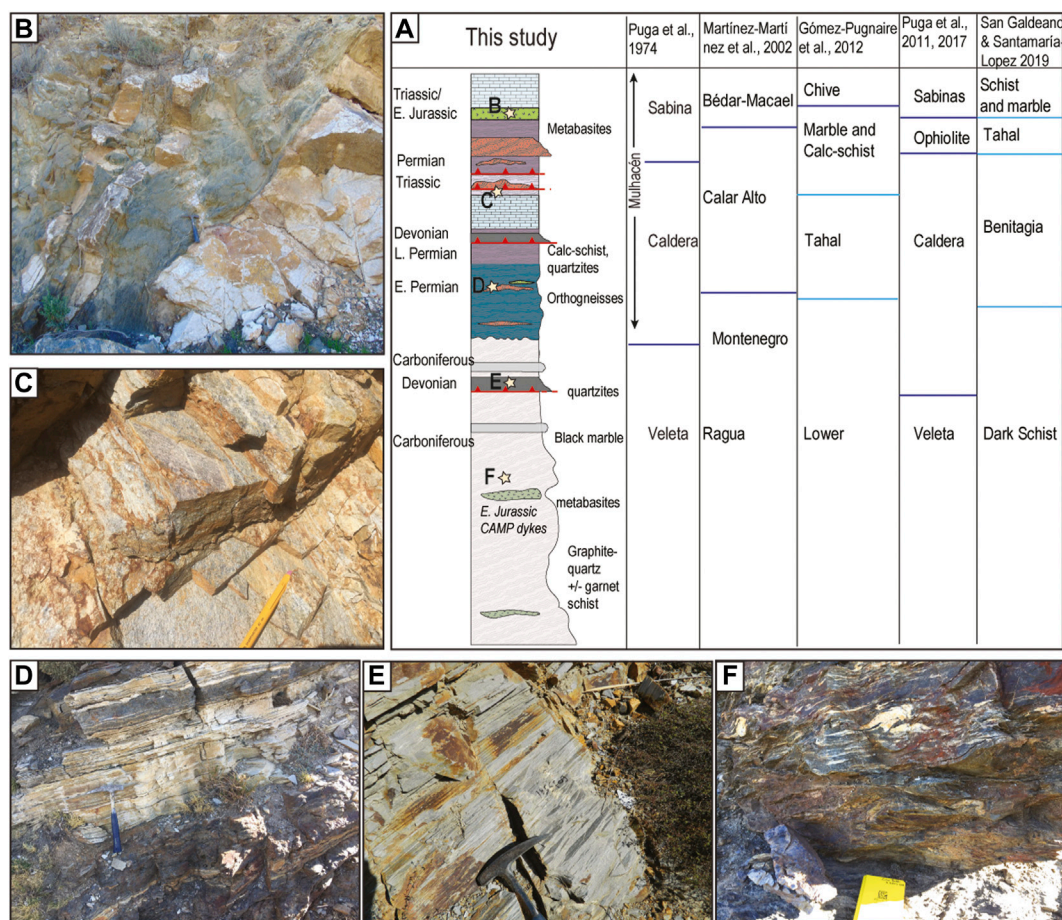
FIGURE 2
Structural column from the NFC including interpretations in this study, previous subdivisions, and sample pictures from the different structural levels. NFC subdivisions from previous studies were compiled from Sanz de Galdeano & Santamaría-López, (2019). **(B)** Metabasites/marble contact from the upper parts of the Mulhacén succession, **(C)** Triassic light garnet mica schist, **(D)** Permian orthogneiss bodies intercalated among garnet mica schist, **(E)** Devonian quartzites, and **(F)** graphitic mica schist from the Veleta unit.

Pugnaire et al., 2004; Platt et al., 2006; Gómez-Pugnaire et al., 2012; Kirchner et al., 2016). The lack of detailed provenance constraints, however, has made it challenging to distinguish between these alternative tectonic models.

2.2 Stratigraphy and geochronology of the nevado-filábride complex

Within the NFC, there is significant disagreement among previous studies regarding stratigraphic subdivisions and correlations, resulting in vastly different stratigraphic schemes with different names and numbers of subdivisions and differing reasoning for the distinction between subunits (Figure 2A). Division of the NFC has been primarily based on the metamorphic record, lithologies, and/or tectonic contacts. Puga et al. (2002) separated the NFC into a lower homogeneous Veleta member and an upper, more

heterogeneous Mulhacén member, which includes metamorphosed mafic and ultramafic rocks. Martínez-Martínez et al. (2002) proposed that the NFC is composed of at least three distinguishable units based on the metamorphic grade, the Veleta/Ragua, the Calar Alto, and the Bédar-Macael units composed of Paleozoic schists and Permian meta-granites (e.g., Augier et al., 2005b; Sanz de Galdeano et al., 2016). More recently, DZ and petrographic evidence from Sanz de Galdeano and Santamaría-López (2019) reported the NFC consists of a lower (3,600 m thick) unit and upper (2,000 m thick) unit with no prominent tectonic contacts. Puga et al. (2002, 2011, and 2017) suggested that ultrabasic rocks represent Jurassic ophiolitic material formed in a new oceanic basin. In contrast, Jabaloy-Sánchez et al. (2015) and Laborda-López et al. (2018) argued that the ultramafic rocks represent mantle peridotites exhumed along a continental margin or ocean basin setting and were later accreted to the Iberian margin.

Traditionally, the NFC has been considered to be a Paleozoic sequence with the stratigraphically uppermost parts being Permo-Triassic. However, this notion has been largely based on correlations with the Alpujárride Complex (Kozur et al., 1974). The first absolute geochronologic data for the NFC were established on the basis of Middle Devonian fossils in marble (Lafuste & Pavillon, 1976; Laborda-López et al., 2015a; Laborda-López et al., 2015b). Later, Gómez-Pugnaire et al. (2012) used U-Pb SHRIMP techniques to date magmatic zircons and documented early Permian ages from six orthogneisses. As these dated samples were from the uppermost stratigraphic section, they concluded the entire NFC sequence must be Paleozoic or older and argued it may have formed along the Central Iberian Zone of the Iberian Massif based on the similarity of the granitoids. Rodriguez-Cañero et al. (2018) assigned the NFC to the Cantabrian Zone of the Iberian Massif, by correlating the NFC conodont fauna with that of the Cantabrian Zone. More recently, studies have supported the scenario that the NFC is a Paleozoic sequence, as Santamaría-López and Sanz de Galdeano (2018) found that the Veleta unit is Carboniferous and reported a single Permian grain age for the Mulhacén unit, arguing for deposition between 349 and 282 Ma. Jabaloy-Sánchez et al. (2018) and Jabaloy-Sánchez et al. (2021), using DZ U-Pb analyses from Sierra de Los Filabres, defined depositional ages spanning from Upper Carboniferous to Early Permian. The existing constraints from these different studies are sparse spatially and stratigraphically disperse throughout the NFC. High-density, stratigraphically integrated sampling, and methodologically consistent geochronologic analyses are needed in order to establish a robust and reliable age framework for the NFC.

2.3 Stratigraphy and geochronology of the Alpujárride Complex

The Alpujárride complex spans the entire Betic Cordillera along the coast of southern Spain and, similarly to the NFC, its internal stratigraphic subdivisions vary from study to study (e.g., Sanz de Galdeano et al., 1997; Alonso-Chaves & Orozco, 2007). Overall, these units span from Permian light schist and phyllites to Triassic platform carbonates, which overlie Carboniferous graphite schist and granitoid basement affected by the Variscan orogeny (Montel, 2000; Rossetti et al., 2010, 2020; Sánchez-Navas et al., 2017; Gómez-Pugnaire et al., 2019). The Eastern Alpujárride contains the lowest stratigraphic and structural levels and is composed mostly of phyllites, quartzites, and carbonates with estimated P/T conditions of 450–480°C and 9–10 kbar (Azañòn & Goffé, 1997). There is an apparent increase in the metamorphic grade from lower to upper units and from east to west (Azañòn et al., 1994). Recently, Jabaloy-Sánchez et al. (2021) and Esteban et al. (2022) have published the first DZ U-Pb data from the Alpujárride complex, showing similar age signatures for the Alpujárride and NFC and

suggesting they may have been deposited in the same or adjacent basins and sourced from the same basement uplifts. The central part of the Alpujárride also contains the Cabezo Blanco orthogneisses that have been dated as Early Permian in age (Zeck and Whitehouse, 1999).

The Eastern Alpujárride in the Sierra de Gádor-Turón area is divided into the lower metasedimentary section characterized by intercalations of pelites and sandstones and thought to be Middle Triassic in age (Perrone et al., 2006; Martín-Rojas et al., 2009). Overlying the metasedimentary succession is a 1,300 m-thick (meta) carbonate succession (Martín-Rojas et al., 2009, 2012) that has been distinguished on the basis of fossils and syn-depositional tectonic features (Delgado et al., 1981). This metacarbonate stratigraphy contains field evidence of extensional growth and syn-depositional normal faulting linked to Triassic rifting (Martín-Rojas et al., 2009). At present day, the Alpujárride and NFC outcrop belt represents a series of large E–W elongated anticlines across four mountain ranges along the south coast of Spain: Sierra Nevada, Sierra Alhamilla, Sierra de los Filabres, and Sierra de la Contraviesa (Figure 1; García-Dueñas et al., 1992). These structures were originally formed by Late Neogene shortening and more recently bound and exhumed due to core-complex-like extensional doming.

3 Methods and results

3.1 Zircon U-Pb geochronology

This study presents zircon U-Pb ICP-MS analyses from 87 metasedimentary and six orthogneiss samples from the NFC and Eastern Alpujárride to reconstruct the initial stratigraphy, provenance, and paleogeography of the Internal Betics. Samples were separated following standard mineral separation procedures, including crushing and grinding, water table preconcentration, and magnetic and chemical density separations. For the U-Pb zircon analyses, 140 grains for detrital and 60 grains for magmatic samples were analyzed by laser-ablation inductively coupled plasma-mass spectrometry (LA-ICP-MS) depth-profiling, following procedures of Marsh & Stockli (2015). GJ1 was used as the primary zircon standard (601.7 ± 1.3 Ma; Jackson et al., 2004) and Plešovice (337.1 ± 0.4 Ma; Sláma et al., 2008) as a secondary standard. We performed data reduction by using IgorPro-based Iolite 3.4 software (Paton et al., 2010) with the VisualAge data reduction scheme (Petrus & Kamber, 2012) and data visualization with detritalPy (Sharman et al., 2018). For zircon ages older than 850 Ma the discordance filter for $^{206}Pb/^{207}Pb$ was set at 30%. For ages younger than 850 Ma, the discordance filter was 15% $^{206}Pb/^{238}U$ vs. $^{207}Pb/^{235}U$ and 10% error filter for $^{206}Pb/^{238}U$ ages, and all ages are reported with two-sigma propagated error. No common Pb correction was applied due to the isobaric interference with ^{204}Hg.
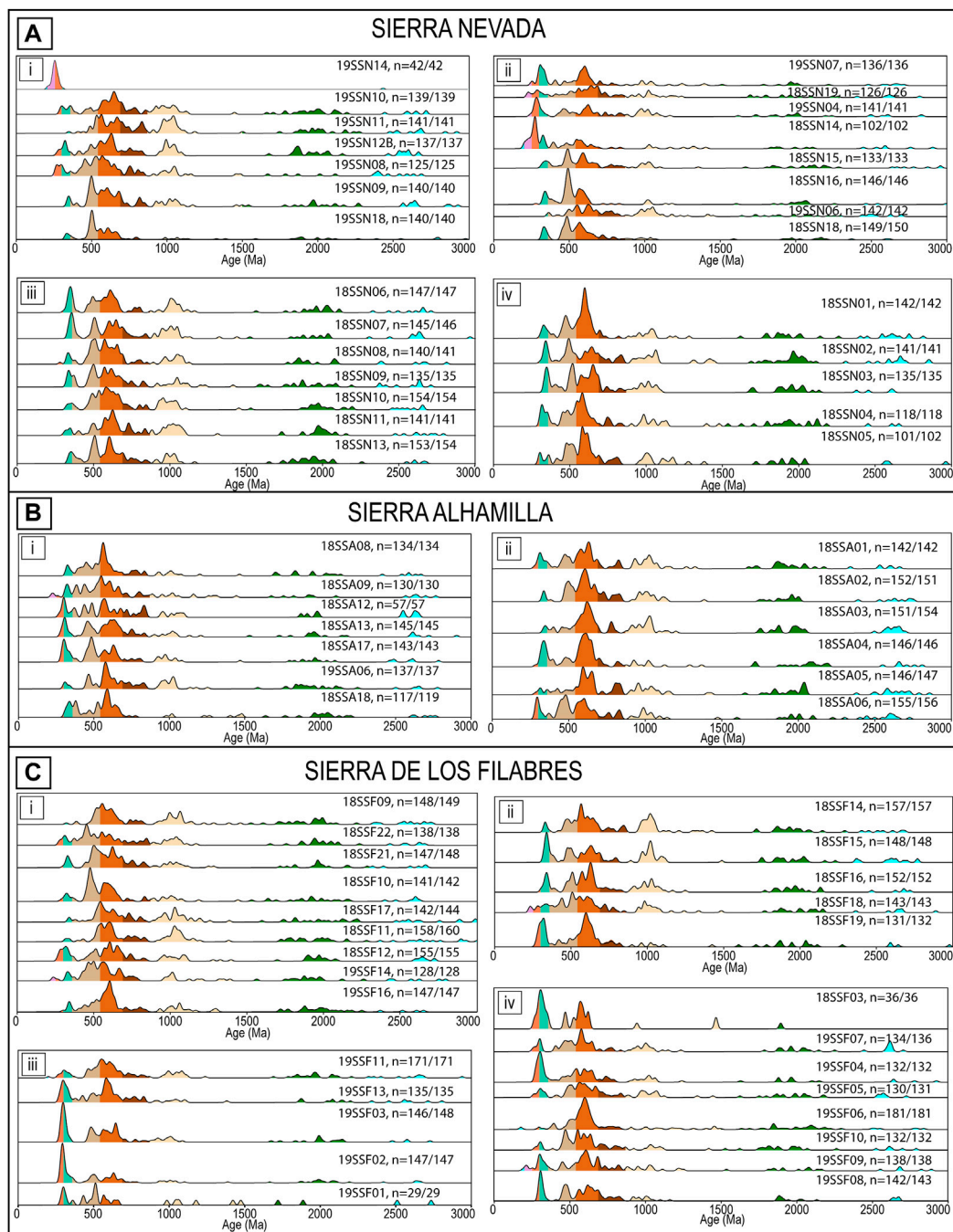
FIGURE 3
Kernel density estimate plots showing the detrital zircon spectrum of individual samples from the NFC organized by their structural position from **(A)** Sierra Nevada, **(B)** Sierra de Los Filabres, and **(C)** Sierra Alhamilla. Colors highlight the different age modes (light blue: Jurassic, pink: Triassic, orange: Permian, light green: Carboniferous, light brown: Early Paleozoic, burnt orange: Ediacaran, dark brown: Early Neoproterozoic, beige: Mesoproterozoic (1,000−1,600 Ma), green: Paleoproterozoic, and cyan: Archean). N = #/# shows the number of zircon grains appeared on the KDE space vs. analyzed and passed the discordance filters.

We systematically collected samples from all the stratigraphic levels from the NFC across Sierra Nevada, Sierra Alhamilla, and Sierra de Los Filabres. We analyzed a total of 72 samples, including

29 samples from the NFC in Sierra Nevada, 15 samples from Sierra Alhamilla, and 28 samples from Sierra de Los Filabres (Figure 1A). These new data help create a new and robust chronostratigraphic

FIGURE 4
Kernel density estimate plots showing the detrital zircon spectrum of individual samples from the Alpujárride Complex organized by lithology; **(A)** graphite mica schist and **(B)** Phyllites and light schist. Colors highlight the different age modes (light blue: Jurassic, pink: Triassic, orange: Permian, light green: Carboniferous, light brown: Early Paleozoic, burnt orange: Ediacaran, dark brown: Early Neoproterozoic, beige: Mesoproterozoic (1,000−1,600 Ma), green: Paleoproterozoic, and cyan: Archean). N = #/# shows the number of zircon grains appeared on the KDE space vs. analyzed and passed the discordance filters.

and provenance framework for the NFC and establish its paleogeographic evolution from Carboniferous to Jurassic. Additionally, 21 samples from the Eastern Alpujárride (Figure 1) are used for a provenance comparison with the NFC and provide additional constraints on their paleogeographic relationship. For the following data presentation, we exclude all Cenozoic zircon metamorphic overgrowths, readily apparent in the depth-profile analyses, as they are not the focus of this study. Supplementary Table S1 contains sample names, location, lithologies, and provenance statistics. Figures 3, 4 as well as Supplementary Table S2 present the individual DZ spectra for all metasedimentary samples, and Figure 5 shows Concordia diagrams from the orthogneisses.

3.1.1 Nevado-Filábride Complex: Sierra Nevada

The West Central transect Figure 3A (i) in the NFC in the Sierra Nevada spans from the peak of Veleta to east of Canales and cuts through all units of the NFC. The structurally lowest samples—two graphite, quartz mica schists (19SSN18 and 19SSN09) —were collected from the Veleta unit and exhibited a similar DZ spectrum ($N = 2$; $n = 281$) with Carboniferous youngest age modes ($n = 14$, ~5%) and detrital age modes in the Early Paleozoic ($n = 84$, 22%–37%), Ediacaran ($n = 88$, 29%–33%), E. Neoproterozoic ($n = 18$, 4%–9%), Mesoproterozoic (31, 6%–

15%), Paleoproterozoic (29, 9%–11%), and Archean (17, 4%–7%). Structurally higher in this transect, we collected five samples from the Bédar-Macael and Tahal units. The lowest portion of both units consists of quartz mica schist (19SSN12B, $n = 137$) with Permian ($n = 4$, 3%), Carboniferous ($n = 10$, ~7%), and age modes at Early Paleozoic ($n = 17$, 12.4%), Ediacaran ($n = 36$, 26%), E. Neoproterozoic ($n = 15$, 10%), Mesoproterozoic (24, 17%), and Paleoproterozoic (20, 15%), and Archean (7, 5%) age modes. These strata are intruded by a tourmaline-bearing orthogneiss (19SSN12 A) with a mean age of 279 ± 1 Ma (Figure 5A). When 86% of the zircon grains are Permian in age for the orthogneiss sample, 14% of the zircon grains represent inherited components with grains from Early Paleozoic to Early Neoproterozoic. Moving to structurally higher levels, we found a quartzite (19SSN11, $n = 141$) with a single youngest Carboniferous grain ($n = 1$, 0.7%) and detrital age modes from Devonian to Archean, including Early Paleozoic ($n = 16$, 12.4%), Ediacaran ($n = 36$, 26%), E. Neoproterozoic ($n = 15$, 10%), Mesoproterozoic (24, 17%), Paleoproterozoic (20, 15%), and Archean (7, 5%). A garnet quartz schist (19SSN10, $n = 139$) overlays this sequence and exhibits a cosmopolitan DZ spectrum including Permian ($n = 2$, 1%), Carboniferous ($n = 7$, 5%), Early Paleozoic ($n = 17$, 12.4%), Ediacaran ($n = 36$, 26%), E. Neoproterozoic ($n = 15$, 10%), Mesoproterozoic (24, 17%) and Paleoproterozoic (20, 15%), and
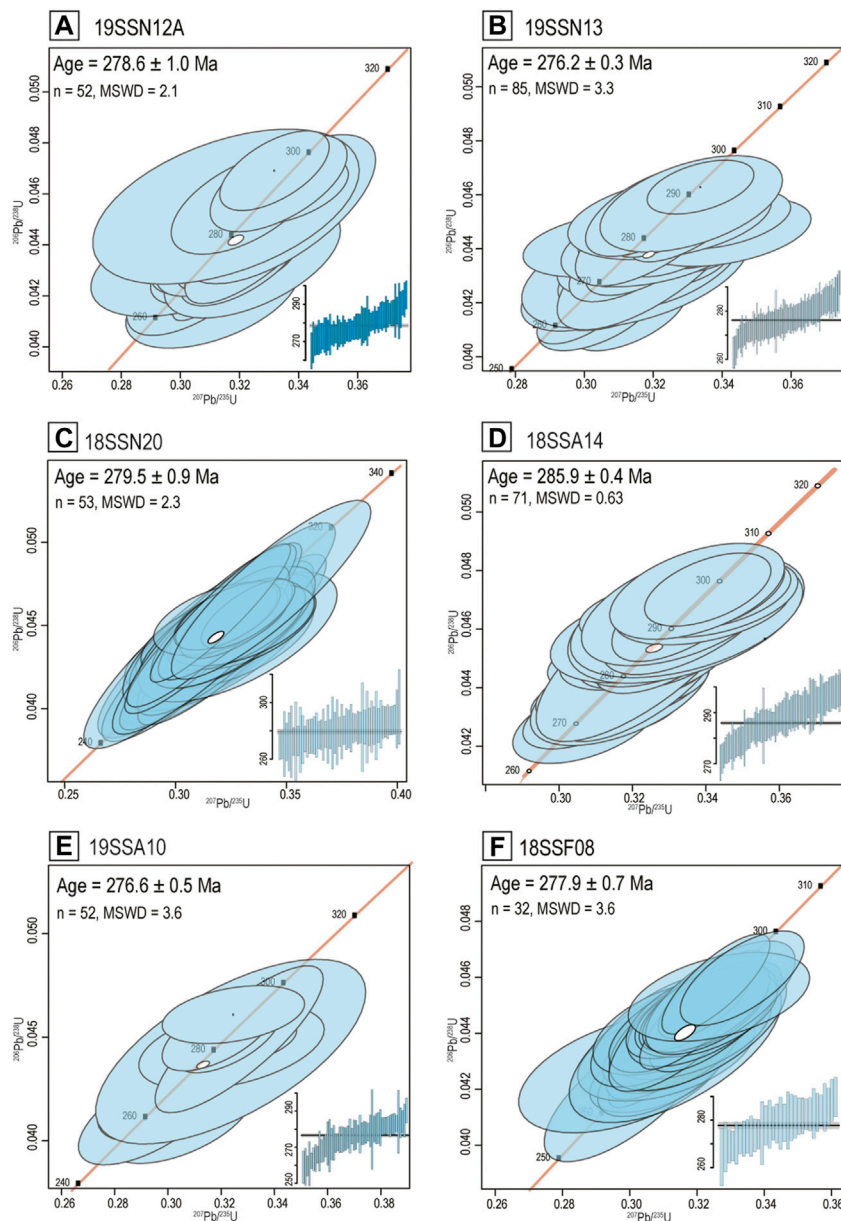
FIGURE 5
Crystallization ages and mean squared weighted deviation (MSWD) calculated by the weighted mean of concordant $^{206}Pb/^{238}U$ ages for analyses from orthogneisses within the Nevado-Filábride Complex.

Archean (7, 5%). At the structurally highest levels of the unit, we sampled an orthogneiss (19SSN13) with a mean age of 276 ± 1 Ma (Figure 5B) with very few (~1%) of the zircon population being inherited ages.

The Southwest transect Figure 3A (ii) in the Sierra Nevada, south of Trevélez, spans all the units in the NFC. Three samples within the Veleta (from structurally lower to higher 18SSN18, quartz, mica metasandstone; 18SSN16, graphite quartz mica schist; 18SSN15, graphite mica quartz schist) show similar DZ

records ($N = 3$, $n = 429$) with youngest ages in the Carboniferous ($n = 41$, 7%–11%) and Early Paleozoic ($n = 148$, 26%–46%), Ediacaran ($n = 118$, 25%–32%), E. Neoproterozoic ($n = 26$, 2%–9%), Mesoproterozoic (35, 5%–14%), Paleoproterozoic (46, 7%–15%), and Archean (14, 2%–5%) detrital age modes. Structurally, in between 18SSN16 and 18SSN15 is a biotite quartz mica schist (19SSN06, $n = 142$) with a different DZ record, containing a single young grain in the Carboniferous ($n = 1$, 0.7%) and detrital age groups in the Early Paleozoic ($n = 19$, 13%), Ediacaran ($n =$

37, 26%), E. Neoproterozoic ($n = 18$, 13%), Mesoproterozoic (40, 28%), Paleoproterozoic (16, 11%), and Archean (11, 8%). Structurally above, four light quartz mica calcite schist samples ($N = 4$, $n = 505$) yield Jurassic–Triassic youngest ages ($n = 21$, 2%–11%) and detrital age modes spanning the Permian ($n = 59$, 4%–23%), Carboniferous ($n = 55$, 5%–20%), Early Paleozoic ($n = 69$, ~12%), Ediacaran ($n = 121$, 15%–30%), E. Neoproterozoic ($n = 38$, 3%–11%), Mesoproterozoic (72, 9%–20%), Paleoproterozoic (44, 7%–10%), and Archean (26, ~5%). The uppermost NFC sample in this transect a tourmaline-bearing orthogneiss (18SSN20) yielded a mean age of 280 ± 1 Ma (Figure 5C).

The Central transect Figure 3A (iii) in the Sierra Nevada spans from La Calahorra to Laroles (Figure 1) and samples exclusively the Veleta unit. This transect cuts through the axis of the large anticline with structurally higher rocks being on the northern and southern flanks of the Sierra Nevada range. Seven graphite quartz mica (garnet) schists (18SSN06, 18SSN07, 18SSN08, 18SSN09, 18SSN10, 18SSN11, and 18SSN13; $N = 7$, $n = 1,018$) from this transect exhibited a cosmopolitan DZ record with youngest ages in the Carboniferous ($n = 51$, 5%–12%), and are characterized by detrital age modes in Early Paleozoic ($n = 116$, ~16%–25%), Ediacaran ($n = 166$, ~18%–44%), E. Neoproterozoic ($n = 39$, ~8%), Mesoproterozoic (182, 13%–23%), Paleoproterozoic (135, 8%–18%), and Archean (60, ~4%–7%) ages. The N–S transect in the Central-East Figure 3A (iv) part of Sierra Nevada spans from Abla to Ohanes (Figure 1) and goes through the Veleta unit. Similar to the previous transect, samples were collected perpendicular to the main foliation and the anticline axes; hence, the uppermost samples stem from the southern and northern edges of the Sierra Nevada. The samples from this transect are quartz mica graphite (garnet) schist (18SSN01, 18SSN02, 18SSN03, 18SSN04, and 18SSN05; $N = 5$, $n = 576$), and they all show a similar age distribution, spanning from Carboniferous (51, 5%–12%), Early Paleozoic ($n = 116$, ~17%–25%), Ediacaran ($n = 39$, ~7%), E. Neoproterozoic ($n = 83$, ~8%), Mesoproterozoic (92, 13%–17%), Paleoproterozoic (85, 9%–17%), and Archean (23, ~2%–9%) ages.

3.1.2 Nevado-Filábride Complex: Sierra Alhamilla

We collected and analyzed seven samples from the Central transect in Sierra Alhamilla which spans from southwest of Turrillas across the Veleta and Bédar-Macael units (Figure 3B (i)). The structurally lowest two samples, overlain by carbonates, are a micaceous metasandstone (18SSA18) and a graphite mica schist (19SSA06), which exhibit similar age modes ($N = 2$, $n = 255$) in Carboniferous (22, 5%–13%), Early Paleozoic ($n = 45$, ~11%–25%), Ediacaran ($n = 82$, 32%), E. Neoproterozoic ($n = 21$, ~2%–13%), Mesoproterozoic (35, 8%–19%), Paleoproterozoic (38, 9%–17%), and Archean (12, ~4%) ages. Atop the carbonates, three mica schist (18SSA17, 18SSA13, 18SSA12) samples exhibited similar DZ records as the structurally lower samples but with the addition of younger

Permian age modes. The combined DZ record ($N = 3$, $n = 345$) of these quartz mica schist shows age signatures with Permian ($n = 18$, ~5%), Carboniferous (38, ~12%), Early Paleozoic ($n = 75$, ~18%–27%), Ediacaran ($n = 82$, ~32%), E. Neoproterozoic ($n = 21$, ~2%–13%), Mesoproterozoic (35, 8%–19%), Paleoproterozoic (38, 9%–17%), and Archean (12, ~4%) detrital ages. Moving upsection in this transect, an orthogneiss (18SSA14) yielded a mean age of 285 ± 1 Ma (Figure 5D).

A transect from the eastern end of Sierra Alhamilla spans from El Saltador to Tristanes (Figure 1) and comprises five Veleta and two Bédar-Macael samples (Figure 3B (ii)). The structure of Sierra Alhamilla is an open anticline with structurally deeper samples in the core. From the structurally higher part of the stratigraphy in the north and toward the center of the anticline to the south, five samples (18SSA01, 18SSA02, 18SSA03, 18SSA04, and 18SSA05, $N = 5$, $n = 683$) yield very similar age signatures with two single Permian grains (2, 2%–0%) and Carboniferous (46, ~15%–3%), Early Paleozoic (82, ~9%–15%), Ediacaran (229, ~29%–40%), E. Neoproterozoic (58, ~6%–15%), Mesoproterozoic (120, 8%–21%), Paleoproterozoic (92, 12%–14%), and Archean (52, ~4%–12%) DZ age modes. In the uppermost part of the stratigraphy in the south, a light quartz mica schist (18SSA06, $n = 156$) exhibits a DZ age spectrum with age modes in the Permian (9, 6%), Carboniferous (8, ~5%), Early Paleozoic (39, ~25%), Ediacaran (39, ~25%), E. Neoproterozoic (14, ~9%), Mesoproterozoic (20, 12%), Paleoproterozoic (12, ~8%), and Archean (15, ~10%) ages. Atop the quartz mica schist, a tourmaline-bearing orthogneiss (19SSA10, $n = 62$), yields a mean age of 277 ± 1 Ma (Figure 5E). Two samples from the west Sierra Alhamilla east of the Baños de Sierra Alhamilla (18SSA08, 18SSA09) gave similar DZ spectra ($N = 2$, $n = 264$) with zircons from the Triassic/Jurassic (3, 2%), Permian (1, < 1%), Carboniferous (20, ~7%), Early Paleozoic (71, ~25%), Ediacaran (70, ~25%), E. Neoproterozoic (48, ~17%), Mesoproterozoic (20, 12%), Paleoproterozoic (23, ~8%), to Archean (11, ~5%) ages.

3.1.3 Nevado-Filábride Complex: Sierra de los Filabres

In Sierra de Los Filabres, we collected samples from three continuous transects in the eastern, central, and western parts of the mountain range. The first transect spans from Escúllar to Los Olmos (Figure 4C (i)) and cuts through the Veleta and Bédar-Macael units. At the southern part of Sierra de Los Filabres, a micaceous metasandstone (18SSF09, $n = 149$) exhibited a DZ age spectrum with the youngest age mode in the Early Paleozoic (20, 13%) and detrital ages in Ediacaran (43, ~29%), E. Neoproterozoic (9, ~6%), Mesoproterozoic (36, 24%), Paleoproterozoic (26, ~17%), and Archean (14, ~9%) periods. Moving stratigraphically down section, a mica graphite garnet-bearing quartz mica schist (18SSF22, $n = 138$) has youngest ages in the Permian and a cosmopolitan DZ spectrum from the Carboniferous (8, ~6%), Early Paleozoic (37, ~27%), Ediacaran (26, ~19%), E. Neoproterozoic (15, ~11%), Mesoproterozoic (22, 16%), Paleoproterozoic (20, ~15%), to

Archean (6, ~4%) ages. Moving up-section, a succession from graphite mica-schist to quartz phyllite (18SSF21, 18SSF10, 19SSF17, and 18SSF11, N = 4, n = 594) exhibits similar age modes in the Carboniferous (26, ~2%–7%), Early Paleozoic (110, ~6–30%), Ediacaran (166, ~25–30%), E. Neoproterozoic (n = 54, ~4%–11%), Mesoproterozoic (116, ~12%), Paleoproterozoic (79, ~10%–15%), and Archean (42, ~4%–9%) ages. In the uppermost portion of the stratigraphy, at the north part of the anticline, a light quartz mica schist (18SSF12, n = 155) has youngest ages in the Permian (n = 9, ~6%) and a cosmopolitan spectrum from Carboniferous (16, ~10%), Early Paleozoic (n = 23, ~15%), Ediacaran (44, ~28%), E. Neoproterozoic (13, ~8%), Mesoproterozoic (23, ~12%), Paleoproterozoic (18, ~12%), to Archean (9, ~6%) ages.

The second transect, in the Central Sierra de Los Filabres, spans from south of the Castro de Los Filabres to Tíjola (Figure 3C (ii)) crossing the Veleta unit and Mulhacén successions. From the southern part of the transect and moving down-section toward the north, three chlorite bearing meta-sandstones (18SSF14, 18SSF15, and 18SSF16, n = 457) show similar DZ U-Pb spectra with age modes in the Carboniferous (44, ~4%–14%), Early Paleozoic (71, ~15%), Ediacaran (124, ~30%), E. Neoproterozoic (30, ~8%), Mesoproterozoic (102, ~20%), Paleoproterozoic (61, ~13%), and Archean (25, ~4%–8%) ages. In the uppermost part of the stratigraphy in the northern part of the Sierra de Los Filabres, a light quartz mica schist (18SSF19, n = 132) gives the youngest age mode in the Permian (n = 11, ~8%) and DZ ages spanning from the Carboniferous (18, ~12%), Early Paleozoic (n = 17, ~13%), Ediacaran (49, ~37%), E. Neoproterozoic (9, ~7%), Mesoproterozoic (8, ~6%), Paleoproterozoic (15, ~11%), to Archean (5, ~4%) ages. At the contact with Alpujárride carbonates, a glaucophane garnet quartz schist (18SSF18, n = 143) has youngest ages in the Triassic–Jurassic (n = 4, ~3%) and detrital age modes from Permian (4, ~3%), Carboniferous (9, ~6%), Early Paleozoic (34, ~24%), Ediacaran (35, ~24%), E. Neoproterozoic (n = 11, ~8%), Mesoproterozoic (23, ~16%), Paleoproterozoic (16, ~11%), to Archean (7, ~5%) ages. The third N–S transect spans the eastern Sierra de Los Filabres, north of Cañada de Miralles up to Líjar (Figure 3C (iii)) and spans the Mulhacén succession. Combined DZ ages from five quartz mica schists and metasandstones (19SSF01, 19SSF02, 19SSF03, 19SSF13, and 19SSF11, N = 4, n = 639) yielded age spectra from the Permian (84, ~4%–26%), Carboniferous (74, ~6%–12%), Early Paleozoic (106, ~15%–31%), Ediacaran (169, ~17%–30%), E. Neoproterozoic (40, ~0%–15%), Mesoproterozoic (69, ~16%), Paleoproterozoic (65, ~6%–13%), to Archean (31, ~5%) ages.

In the Lubrín area, samples were collected from the different units exposed (Figure 3C (iv)). A tourmaline-bearing garnet orthogneiss (18SSF08) from the main Lubrín exposure yields a zircon mean age of 280 ± 1 Ma (Figure 5F). A mica garnet gneiss (19SSF07) and a quartz mica schist (19SSF04) show similar DZ records (N = 2, n = 273) with age modes in the Permian (23, ~5%–12%), Carboniferous (29, ~4%–17%), Early Paleozoic (50,

~15%–21%), Ediacaran (71, ~25%), E. Neoproterozoic (18, ~6%), Mesoproterozoic (38, ~13%), Paleoproterozoic (26, ~11%–8%), and Archean (18, ~3%–10%) ages. In La Rambla, we collected three samples; the lower formation with two graphite mica schist (19SSF10 and 19SSF08; N = 2, n = 275) has zircon age modes ranging from the Permian (6, ~2%), Carboniferous (30, ~4%–18%), Early Paleozoic (53, ~19%), Ediacaran (82, ~30%), E. Neoproterozoic (35, ~12%), Mesoproterozoic (26, ~9%), Paleoproterozoic (30, ~7%–15%), to Archean (13, ~4%) ages. The upper formation from this group is a light quartz mica schist (19SSF09, n = 138) with the youngest age mode in Triassic/Jurassic (6, ~4%) and ages spanning from the Permian (84, ~4–26%), Carboniferous (74, ~6%–12%), Early Paleozoic (106, ~15%–31%), Ediacaran (169, ~17%–30%), E. Neoproterozoic (40, ~0%–15%), Mesoproterozoic (69, ~16%), Paleoproterozoic (65, ~6%–13%), to Archean (31, ~5%) ages. In Los Gallardos area, a garnet mica schist (19SSF06, n = 181) shows youngest ages in Early Jurassic (2, ~1%) and DZ modes from Permian (2, ~1%), Early Paleozoic (27, ~15%), Ediacaran (83, ~46%), E. Neoproterozoic (12, ~0%–15%), Mesoproterozoic (18, ~10%), Paleoproterozoic (30, ~16%), to Archean (6, ~3%) ages. As mentioned earlier, a quartz mica schist (19SSF05, n = 131) revealed the youngest age mode in Permian (5, 4%) and similar zircon age spectra in the Carboniferous (8, ~6%), Early Paleozoic (19, ~15%), Ediacaran (40, ~30%), E. Neoproterozoic (12, ~9%), Mesoproterozoic (22, ~17%), Paleoproterozoic (17, ~13%), and Archean (8, ~6%) ages.

3.1.4 Eastern Alpujárride Complex

In addition to the data from the NFC, we collected 21 samples from different stratigraphic levels at the eastern part of the Alpujárride Complex, six samples from Sierra de la Contraviesa, four from the southern flank of the Sierra Nevada, ten from the southern Sierra Alhamilla, and one from Sierra de Los Filabres. In the Sierra Nevada, four samples were collected from the southern part of the range along the contact with the NFC. A graphitic mica schist [Figure 4 (i); 19SSN16, n = 138] south of Laroles exhibits youngest ages in the Carboniferous (5, ~4%), and detrital modes from Early Paleozoic (27, ~20%), Ediacaran (18, ~13%), E. Neoproterozoic (46, ~33%), Mesoproterozoic (17, ~12%), Paleoproterozoic (16, ~12%), to Archean (9, ~7%). Three blue/purple phyllites [Figure 4 (ii); 19SSN16, 19SSN08, and 19SSN17] from the Órgiva area are grouped together due to their similar lithology and DZ record (N = 3; n = 283); even though the sample 19SSN17 contains insufficient zircon (n = 27) for a robust statistical analysis, it preserves similar age modes as the other two samples. From this group, the youngest age mode is Permian (16, 0%–7%) and zircon components are present from the Carboniferous (22, ~6%–17%), Early Paleozoic (65, ~6%–25%), Ediacaran (44, ~6%–19%), E. Neoproterozoic (73, ~26%–40%), Mesoproterozoic (31, ~9%–17%), Paleoproterozoic (20, ~6%–12%), to Archean (12, ~5%) ages. From Sierra de Los

Filabres, one purple phyllite (19SSF15) from Gor only yielded 31 zircon grains with ages in the Permian (1, 3%), Carboniferous (2, ~6%), E. Paleozoic (10, ~32%), Ediacaran (7, 22%), E. Neoproterozoic (5, ~16%), Mesoproterozoic (1, 3%), Paleoproterozoic (4, ~13%), and Archean (1, 3%) ages.

In Sierra Alhamilla, 10 samples were collected from different structural levels along with the contact with the NFC from three main lithologies: graphite mica schist, purple phyllite, and light metasandstone or schist. The graphitic mica schist and chlorite mica schist samples [Figure 3 (i); 18SSA10, 19SSA01, 19SSA07, 19SSA09, 19SSA04, 19SSA05, and 18SSA16] from the Baños De Sierra Alhamilla, south of Colativí and close to Huebro, all exhibit similar DZ ($N = 7$; $n = 1,007$) with youngest ages in the Carboniferous ($n = 84$, ~3%–17%) and detrital age modes spanning from the Early Paleozoic ($n = 175$, ~10%–25%), Ediacaran ($n = 207$, ~20%), E. Neoproterozoic (274, ~20%–33%), Mesoproterozoic ($n = 122$, ~16%), Paleoproterozoic ($n = 122$, ~10%), and Archean (48, ~5%) ages. The leucocratic schist and purple phyllite [Figure 4(ii); 19SSA02, 19SSA03, and 18SSA11] yield a combined DZ record ($N = 3$; $n = 451$) from the Permian (14, ~4%), Carboniferous (29, ~2%–7%), Early Paleozoic (58, ~10%–20%), Ediacaran (79, ~18%), E. Neoproterozoic (153, ~35%), Mesoproterozoic (52, ~13%), Paleoproterozoic (51, ~10%), to Archean ages (15, ~5%).

In Sierra de la Contraviesa, we collected six samples along a transect spanning from La Rábita to Cádiar (Figure 1). Similar to the other regional Alpujárride samples, comparable lithologies yield similar DZ signatures, and hence, we grouped graphitic mica schist and phyllite with light schist. The two graphitic mica schist [Figure 4 (i); 19SSG02 and 19SSG05; $N = 2$; $n = 210$] have youngest ages that are Carboniferous or older and with zircon detrital modes in the Carboniferous (6, ~3%), Early Paleozoic (23, ~10%), Ediacaran (49, ~23%), E. Neoproterozoic (61, ~28%), Mesoproterozoic (20, ~9%), Paleoproterozoic (34, ~13%–17%), and Archean (16, ~6%–10%), while the light schist and phyllite (Figure 4ii; 19SSG01, 19SSG03, 19SSG04, and 19SSG06) exhibit the youngest ages in the Triassic and Permian and the combined DZ age modes ($N = 4$, $n = 475$) from the Triassic (2, ~0%–2%), Permian (28, 4%–8%), Carboniferous (37, ~4%–15%), Early Paleozoic (87, ~16%), Ediacaran (91, ~15%–23%), E. Neoproterozoic (96, ~20%), Mesoproterozoic (46, ~9%), Paleoproterozoic (61, ~13%), to Archean (27 ~2%–9%) ages.

3.2 Apatite U-Pb geochronology

To perform *in situ* apatite U-Pb LA-ICP-MS from a metabasite sample, we collected energy dispersive spectroscopy (EDS) maps from one thin section of the Sierra Nevada to identify apatite grains. We acquired Ca, P, Si, and Ti *via* a scanning electron microscope EDS detector and created element maps (Figure 6A). We subsequently dated the apatite, using 30-μm spots, 200 shots of ablation, 10 Hz, and with MAD

apatite (Thomson et al., 2012, in-house TIMS ages of 472.4 ± 0.7 Ma) as the primary standard and McClure Mountain (523.5 ± 1.5 Ma; Schoene and Bowring, 2006) as a secondary monitor. Apatite data are plotted in Tera-Wasserburg Concordia diagrams (Tera and Wasserburg, 1972; Vermeesch, 2018).

We applied this method to three metabasites from the Mulhacén, Alpujárride, and Veleta units. However, only the metabasite from the Veleta unit contained sufficient uranium to produce a robust geochronometric age, and hence, we only present the results from that sample (19SSN02). The metabasite is intercalated with graphitic mica schist in the southern part of Sierra Nevada (Figure 6C), close to Trevélez. When macroscopically the outcrop does not appear to have foliation, microscopically there is a weak fabric. The metabasite is mostly composed of actinolite, pyroxene, plagioclase, minor quartz, and biotite. Trace phases in the rock revealed by the EDS maps are apatite and titanite. We plotted the data using the Tera–Wasserburg Concordia diagram, in which the lower intersect yields an age of 197 ± 6 Ma and common lead composition of 0.8 (Figure 6B) (Supplementary Table S3).

4 Discussion

4.1 Pre-subduction configuration of the Nevado-Filábride Complex

4.1.1 Chronostratigraphic framework of the Nevado-Filábride Complex

Zircon U-Pb geochronologic constraints have shown that the NFC includes a Paleozoic sequence mainly composed of Carboniferous and Permian rocks (e.g., Jabaloy-Sánchez et al., 2018; Santamaría-López et al., 2019; Jabaloy-Sánchez et al., 2021). In this study, our new chronostratigraphic framework shows that MDAs (see Supplementary Material S1) span from Devonian (or older) to Early Jurassic, preserving a continuous stratigraphic record (Figure 8). The oldest ages in the NFC have Cambrian MDAs and are from quartzites or fine-grained meta-sandstones (Figure 7E). Individual zircon grain ages show a profile from Cambrian toward Devonian/Carboniferous which might be attributed to a lead loss event during the Early Paleozoic in response to Variscan metamorphism (Supplementary Figure S1). However, another important factor to consider is the Devonian fossils that have been found within these strata (Lafuste and Pavillon, 1976). Hence, it is possible that these rocks are Devonian in age, but during their deposition, there were not many active zircon sources available to give a statistically robust Devonian MDA. The lithologies with Cambrian/Devonian MDAs (Figures 2A,E) have been identified in the upper parts of the Veleta/Ragua unit, but we also found them in the lower parts of the Bédar-Macael unit intercalated with rocks with Permian MDAs. Previous work based on the presence of fossils, as well as high sedimentation rates, suggested that the
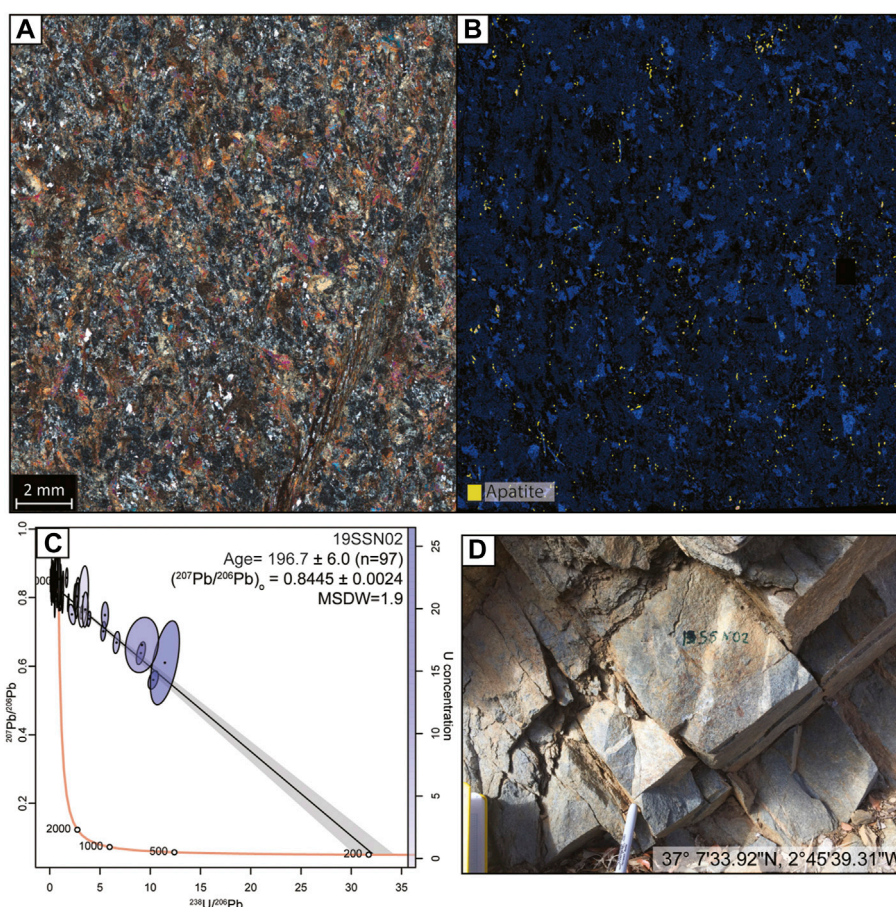
FIGURE 6
(A) Thin section scan from the metabasite (19SSN02) collected from the Veleta unit; **(B)** other half of the thin section scan is shown as an EDS map illustrating the presence of apatite (Phosphorus). **(C)** Tera-Wasserburg diagram of apatite analyses. **(D)** Macroscopic picture of the metabasitic outcrop with sample coordinates; the exact location is also indicated on Figure 1.

units were deposited within a closed marine shelf environment (Laborda-López et al., 2015a).

The Carboniferous strata dominate the exposed NFC and form a monotonous sequence of graphite, quartz, mica (±garnet) schist intercalated with quartzites, metabasitic lenses, and black marble at higher parts of the stratigraphy (Figures 2A,F). This sequence is predominantly exposed along the anticlinal axes of Sierra Nevada, Sierra de Los Filabres, and Sierra Alhamilla (Figure 1). The thickness of this section has been estimated at ~3.5–4 km based on the average dip direction (e.g., Sanz de Galdeano and Santamaría-López, 2019). In addition, this succession preserves sedimentary structures and fossils within the Veleta and Montenegro Carboniferous rocks (Jabaloy et al., 1993; Rodriguez-Cañero et al., 2018), indicating less pervasive deformation during Cenozoic subduction. Most of the Early Permian strata are dominated by graphite schist interlayered with quartzites, metasandstones, and transitioning into light schist at the upper parts of the stratigraphy. Together with

Permian orthogneisses, they are part of the Bédar-Macael unit that outcrops at higher levels of the structural column (Figures 2A,D). In south Sierra de Los Filabres, we have also identified sedimentary structures preserved within meta-sandstones (cross-beds in metasandstone; Figure 7B). Notably, orthogneisses have only been mapped within the Mulhacén succession and are absent from the Veleta/Montenegro units.

The Late Permian to Early Jurassic strata is more heterogeneous with white and dark schist and variable amounts of quartz, mica, glaucophane, kyanite, garnet, etc. (Figures 2A,C, 6). This stratigraphic/structural succession is the so-called Calar-Alto unit, which also includes the Tahal formation. Late Permian-Early Jurassic MDAs are only observed in the structurally middle section of the NFC, intercalated with Permian rocks along the southern and western edges of Sierra Nevada and the eastern and western flanks of Sierra de Los Filabres. Our *in situ* apatite analyses from a metabasitic sample within the Carboniferous strata in the Veleta
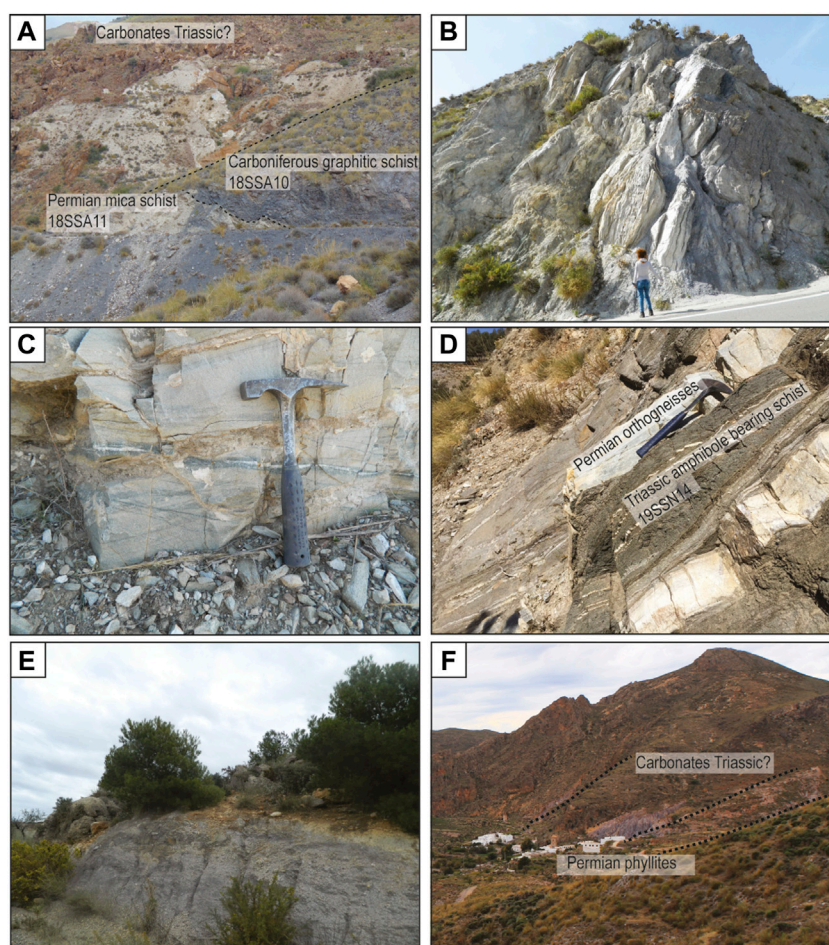
FIGURE 7
(A) Outcrop in Sierra Alhamilla from the Alpujárride Complex, showing Permian mica schist overlaying the Carboniferous graphitic schist. **(B)** Talc/serpentinite outcrop marking the contact between the NFC and Alpujárride in south Sierra Nevada. **(C)** Permian metasandstone from south Sierra de Los Filabres possibly preserving cross-bedded strata from initial deposition. **(D)** Permian orthogneiss overlaying the Triassic amphibolite on West Sierra Nevada. **(E)** Carboniferous graphitic mica schist underlaying carbonates in the middle Sierra Alhamilla. **(F)** Outcrop of East Sierra Alhamilla from the Alpujárride complex showing thrust sheets of Permian phyllites with overlaying Triassic (?) carbonates.

unit revealed an age of 197 ± 6 Ma (Figure 6C). The mineralogical assemblage of this rock is actinolite hornblende, quartz, and plagioclase, suggesting low-grade greenschist metamorphism. The pre-Cenozoic age shows that apatite within the metabasite has not been reset or recrystallized during subduction-related metamorphism. Hence, this age is likely a cooling apatite age and signifies the magmatic emplacement of the dyke. The cooling of these dykes must be contemporaneous with the deposition of the youngest Triassic/Jurassic NFC sedimentary strata. Zircon grains from the Triassic/Jurassic population are limited to ~3–5 grains per sample. However, this age population is consistent throughout the region within the Tahal formation, and Triassic individual zircon grains have also been identified in previous studies but were not in statistically robust numbers to count toward MDA calculations (Jabaloy-

Sánchez et al., 2018; Santamaría-López and Sanz de Galdeano, 2018; Jabaloy-Sánchez et al., 2021). Sample 19SSN14 (Figures 3A,7D) (i) displays a distinct unimodal peak in Late Permian/Triassic with fewer and smaller size zircon (*n* = 42); thus, infertility of zircon and abundant amphibole may indicate a more mafic composition and suggest that this lithology is related to Triassic rifting.

In the uppermost parts of the structural column in the Mulhacén succession, we found metabasitic and meta-ultramafic rocks (Figure 2A). Our attempt to date the apatite grains from these lithologies was not successful since there was little uranium and high concentrations of common lead, likely due to later subduction metamorphism. However, previous workers were able to obtain zircon ages and Rb-Sr isochron ages from the metabasitic rocks outcropping in the Mulhacén
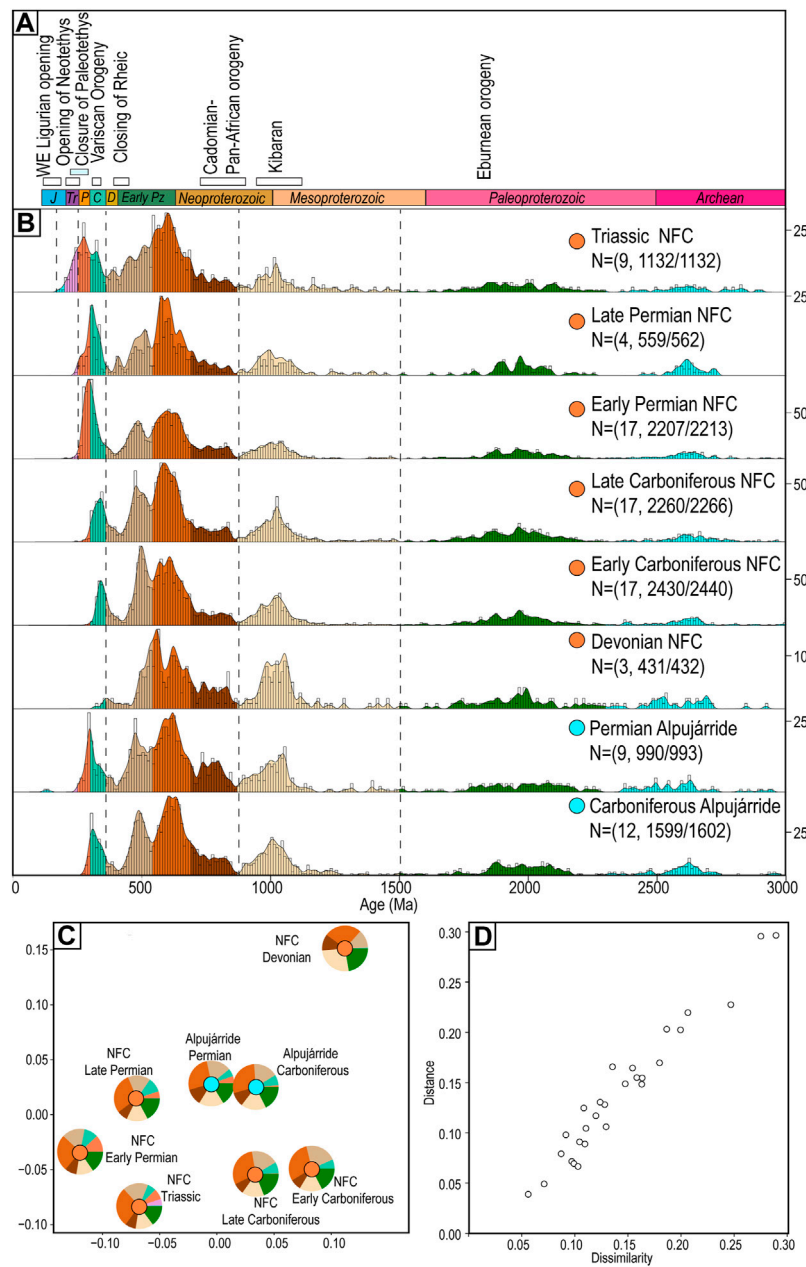
FIGURE 8
(A) Samples from the NFC and Alpujárride plotted in KDEs represent multiple samples grouped based on their extracted maximum depositional ages. Orange circles show NFC samples, while orange circles the Alpujárride samples. **(B)** Multi-dimensional space diagram showing similarity between NFC and Alpujárride spectra grouped by MDAs. **(C)** Shepard plot showing the goodness of best fit for the MDS plot. Colors on KDEs and pie diagrams highlight the different age modes (light blue: Jurassic, pink: Triassic, orange: Permian, light green: Carboniferous, light brown: Early Paleozoic, burnt orange: Ediacaran, dark brown: Early Neoproterozoic, beige: Mesoproterozoic (1,000–1,600 Ma), green: Paleoproterozoic, and cyan: Archean). N = #/# shows the number of zircon grains appeared on the KDE space vs. analyzed and passed the discordance filters.

succession from various localities and the resulting ages span from 146 to 187 Ma (Hebeda et al., 1980; Ferreira et al., 1988; Puga et al., 2002, Puga et al., 2005, Puga et al., 2011). The geologic significance of these metabasitic rocks has been widely debated and led to disagreement about the nature of oceanic domains at this time. The upper marble layers are intercalated with

metabasites in many localities (Figure 7B) and outcrops mostly in eastern Sierra de Los Filabres. It preserves a significant thickness and provides constraints on the depositional environment for this section of the NFC, but there are no age constraints due to the lack of fossils and minerals to provide radiometric ages. However, it has been

proposed that the carbonate sequence in the NFC may be Triassic or younger in age (Sanz de Galdeano et al., 2016).

4.2 Permian magmatism in the Nevado-Filábride Complex

Orthogneisses play an essential role in the NFC not only for the provenance information related to their affinity but also for setting robust age constraints on our chronostratigraphic framework. There are mainly two petrologic types: amphibole-biotite gneisses and leucocratic tourmaline-bearing gneisses. The primary composition is peraluminous granitic to rhyolitic (Gomez-Pugnaire et al., 2004; Gomez-Pugnaire et al., 2012), and they are likely formed during post-orogenic extension signaling the end of the Variscan orogeny. In Sierra Nevada and Sierra Alhamilla, the orthogneisses outcrop as slivers, following the same attributes (foliation and lineation) as the hosting lithologies (Figure 7D). They are observed in multiple structural positions between the Devonian, Permian, and Triassic strata, showing old on top of young patterns. The most significant exposure is found at Sierra de Los Filabres in the Lubrin area where orthogneisses are exposed in the higher stratigraphic section between Triassic strata and intercalated with Permian and Carboniferous strata. In Sierra Alhamilla, orthogneisses are only observed at the highest parts of the stratigraphy at the southern part of the mountain range on top or within the Permian strata. The average age of the quartzo-feldspathic mylonitic orthogneiss is 285 Ma, which is older than the tourmaline-bearing orthogneisses (275–279 Ma; Figure 5). Zircon data from all the orthogneisses in the NFC preserve relict inherited grains. From the total grain population, less than 10% of the zircon grains are older than their crystallization ages, with the most prominent population in the Cambrian but a total age range from 310 Ma to 2 Ga (Supplementary Table S2). These inherited zircon grains suggest either melt contamination during emplacement or they have been assimilated from the host Permian rock.
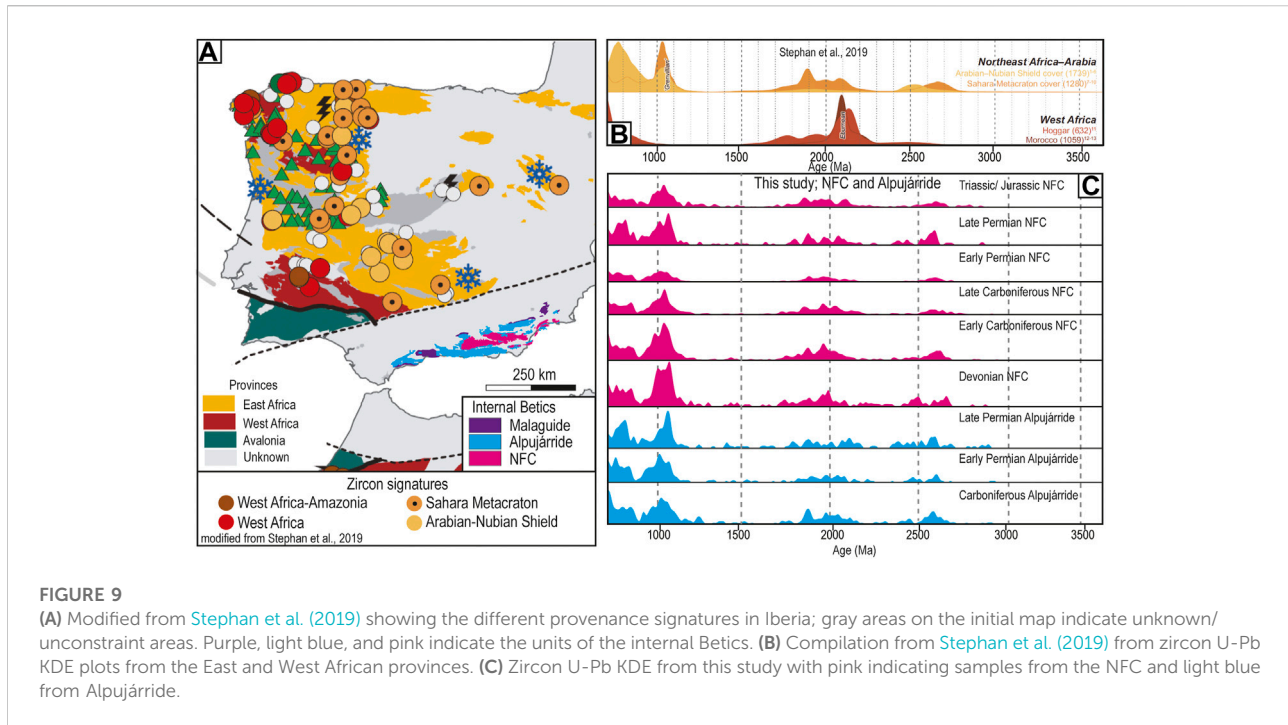
4.3 Provenance and paleogeography of the Nevado-Filábride Complex and synthesis with previous studies

Our geochronological analyses spanning all the different structural and stratigraphic levels of the NFC provide an unprecedented data set to investigate its paleogeographic evolution in the Western Mediterranean. The multidimensional scaling diagram (Figures 8C,D), which represents how dissimilar the samples are in a 2-dimensional plot (Vermeesch, 2013; Spencer et al., 2016; Wissink et al., 2018), shows that the NFC subunits all have remarkably similar provenance age modes. Consequently, even though the NFC strata spans from Devonian to Early Jurassic,

the provenance distribution does not show any major discrepancies in the main zircon populations over time. The only significant changes in DZ spectra are the appearance of younging age modes as new zircon sources become available, lending confidence to our MDA calculation and robustness of our pre-subduction stratigraphic reconstruction. The age modes observed in the NFC are Jurassic (180–200 Ma), Triassic (200–251 Ma), Permian (251–298 Ma), Carboniferous (298–358 Ma), Early Paleozoic (358–541 Ma), Ediacaran (541–635 Ma), Early Neoproterozoic (635–1,000 Ma), Mesoproterozoic (1,000–1,600 Ma), Paleoproterozoic (1,600–2,500 Ma), and Archean (>2,500 Ma) (Figures 3,8). Our distribution of DZ age modes generally agrees well with published zircon data from other studies (Jabaloy-Sánchez et al., 2018; Santamaría-López and Sanz de Galdeano, 2018; Jabaloy-Sánchez et al., 2021) (Figures 8A,B), with an exception that our study reports the first Triassic-Early Jurassic age constraints in the NFC from metasedimentary beds in the Tahal formation.

Paleoproterozoic and Archean populations are less prominent than the other age modes (<~10% for each, Figure 8B). Qualitatively comparing these age modes with the DZ compilation by Stephan et al. (2019), it is clear that the NFC has age modes similar to the Northeast Africa craton rather than the West Africa craton (Figure 10). The large Early Neoproterozoic population is related to the Kibaran/Grenville orogeny and has been observed in many locations of the Iberia Peninsula including Central Iberia, West Astur-Leonian, and Cantabrian zones (e.g., Bea et al., 2010; Cambeses et al., 2015; Fernández et al., 2015). Upper Ordovician sources are attributed to the Early Paleozoic rifting, which separated the Central Iberian, West Astur-Leonese, and Cantabrian zones from Gondwana, while the Ediacaran-Cryogenian peak is attributed to the Cadomian/Pan-African orogeny that contributes to the formation of the Gondwanan supercontinent. Both the Early Paleozoic and Ediacaran-Cryogenian modes expand from 490 to 630 Ma and have been observed in all the samples. The Upper Ordovician, Silurian, and Devonian zircon age populations are attributed to the opening of the Rheic ocean, and evidence of these magmatic intrusions appears in Iberia (Talavera et al., 2013). As previously discussed by Jabaloy-Sánchez et al. (2018), samples collected from the Aulago (Veleta) formation in the NFC populations are absent in the West-Asturian Leonese and Cantabrian, but they could be related with Avalonian terranes and opening of and the volcanic arcs developed during the closure of Rheic Ocean and the collision between Laurussia and Gondwana during Devonian to Early Carboniferous times (Accotto et al., 2021). These zircon age modes are also present in the Rif Cordillera (Azdimousa et al., 2019).

The abundant Carboniferous zircon populations in most samples are related to the abundant granitoids formed during the Variscan orogeny. Sources for these zircon populations are occupying large portions of the Iberia massif including the Central Iberian zone (e.g., Bea et al., 2007; Ribeiro et al., 2019) and a

FIGURE 9
(A) Modified from Stephan et al. (2019) showing the different provenance signatures in Iberia; gray areas on the initial map indicate unknown/ unconstraint areas. Purple, light blue, and pink indicate the units of the internal Betics. **(B)** Compilation from Stephan et al. (2019) from zircon U-Pb KDE plots from the East and West African provinces. **(C)** Zircon U-Pb KDE from this study with pink indicating samples from the NFC and light blue from Alpujárride.

portion of the NFC orthogneisses (Gomez-Pugnaire et al., 2004; Gomez-Pugnaire et al., 2012). The end of the Variscan orogeny was marked by magmatism related to post-orogenic rifting in the Early Permian with extensive crustal thinning (de Saint Blanquat et al., 1990; Vissers, 1992; de Saint Blanquat, 1993; Saspiturry et al., 2019). Magmatism during this period has also been recorded in other parts of the Variscan belt of Iberia, with crystallization ages from Late Carboniferous to Early Permian (Aguado et al., 2005; Bea et al., 2006; Gutiérrez-Alonso et al., 2011; Villaseca et al., 2011). This emplacement of melts is recorded in Central Iberian and West Asturian-Leonese zones by felsic leucogranites (Fernández-Suárez et al., 2000, Fernández-Suárez et al., 2011; Gutiérrez-Alonso et al., 2011) that have similar geochemical signatures as those in the Betic cordillera (Gómez-Pugnaire et al., 2012). These intrusive bodies may have acted as sedimentary sources for the NFC and Alpujárride during this time.

The Late Permian and Triassic sources signify the transition to widespread extension and corresponding syn-rift deposition (Stampfli and Kozur, 2006; Gretter et al., 2013). Triassic ash beds have been extensively dated in the Southern Alps (Storck et al., 2019). During crustal thinning and the creation of new accommodation space, sedimentary deposits have been imaged in the Atlantic and Iberian basins (e.g., Deptuck & Kendell, 2017; Campos-Soto et al., 2019). The culmination of rifting resulted in the opening of the western Alpine Tethys Ocean and the Central Atlantic Ocean (Andrieux et al., 1989; Favre & Stampfli, 1992; Guerrera et al., 1993). When this transition has been documented in syn-rift deposits elsewhere, we reported the first evidence of Triassic–Early Jurassic metasedimentary syn-rift strata within

the Tahal unit of the NFC. Early Jurassic metabasites from this study appear as intrusions within older Carboniferous metasedimentary strata in the Veleta unit. Their timing of crystallization suggests they are likely linked to the opening of Tethys and the mafic magmatism occurring in the region. Previous studies have dated Jurassic metabasites in the Mulhacén unit successions (e.g., Puga et al., 2005). Zircon rims and Ar/Ar on pyroxenites have also yielded Jurassic and Early Cretaceous ages in the Rif Cordillera (Jubrique Unit; Sánchez-Rodríguez and Gebauer, 2000) and have been interpreted to be mantle origin largely contemporary to the magmatic activity we observe in the NFC. Importantly, the lack of ages after the Early Jurassic signifies a depositional hiatus and/or absence of zircon sources between continental breakup and the onset of subduction in the Cenozoic.

4.4 Stratigraphic arrangement and provenance of the eastern Alpujárride complex

The origins of the Paleozoic/Mesozoic strata of the Internal Betics and the relationship among the NFC, Alpujárride, and Iberian massif have been debated due to the lack of dense and consistent geochronometric constraints. Twenty-one samples from Alpujárride were used with the identical methodology for MDA determination as described earlier for the NFC. Along the low-angle normal fault that forms the contact with the NFC in the southern Sierra Nevada and Sierra Alhamilla, Alpujárride units exhibit
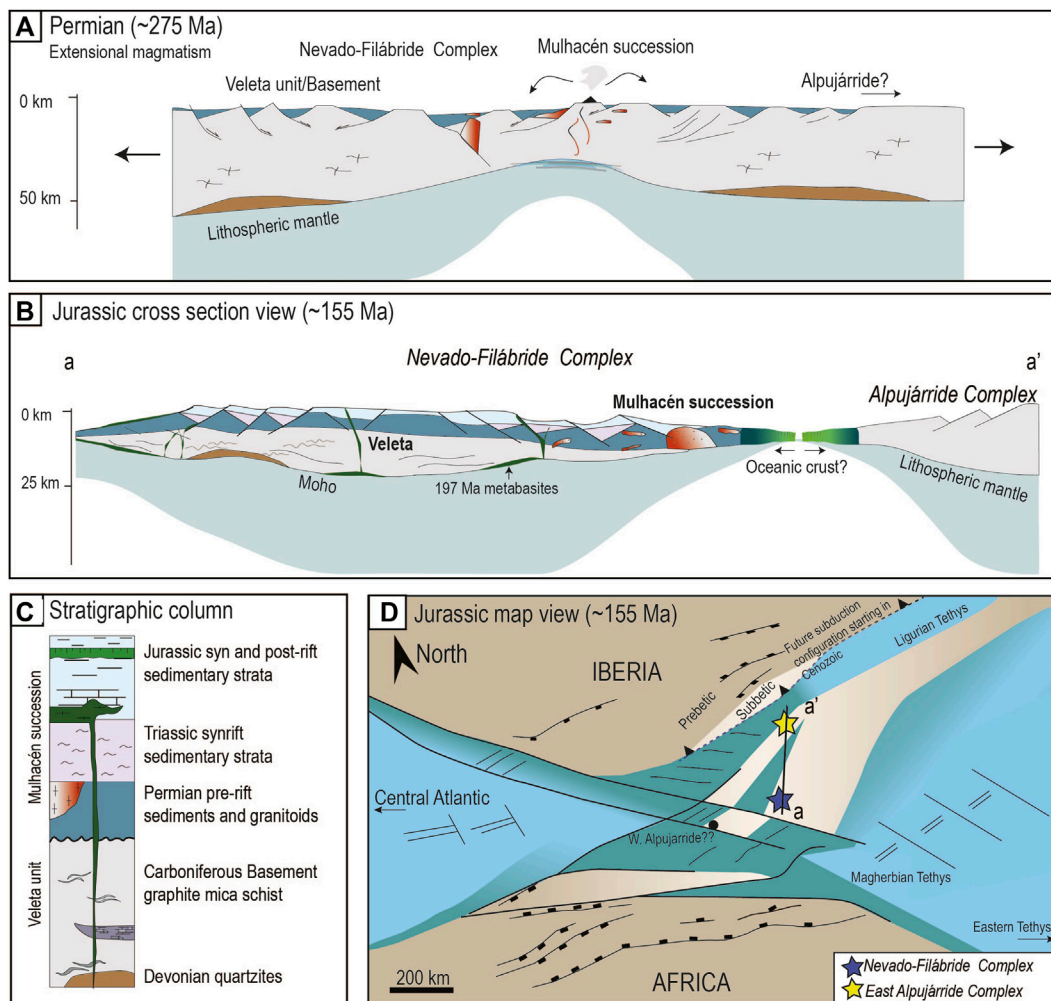
FIGURE 10
(A) Cross section indicating the Permian tectonic configuration for the NFC. **(B)** Cross section indicating the pre-subduction configuration of the NFC and relative position with the Alpujárride complex. **(C)** Stratigraphic column illustrating the pre-subduction stratigraphy of the NFC from the Devonian to Early Jurassic. **(D)** Map view of the Late Jurassic configuration modified after Leprêtre et al. (2018) showing position of the NFC and Alpujárride and the future position of the Cenozoic subduction zone. Dark brown illustrates the continental crust, and light brown hyperextended the continental crust. Light blue illustrates the oceanic domain, while green areas show transitional oceanic domains.

Permian and Carboniferous ages (Figure 4). The graphitic darker mica-schist represents the Carboniferous strata, while the light schist and purple/blue phyllites yield Permian ages. The timing of deposition agrees with previous studies (Jabaloy-Sánchez et al., 2021; Esteban et al., 2022); however, this is the first study that sets exact zircon geochronometric constraints on the different lithologies within the Alpujárride complex with robust MDAs. These lithologies are overlain by Triassic carbonate platforms in most localities, as defined by earlier fossil biostratigraphic correlations (Figure 7A; Martin and Braga, 1987).

In Sierra de la Contraviesa, all the samples from the Adra and Escalate unit are Permian in age (Figures 1,4), while within the Paleozoic Salobreña unit, two graphitic mica schists revealed different MDAs with the structurally higher being Permian and the lowest Ordovician in age. Slivers of Permian and Carboniferous rocks are repetitive across the Alpujárride-NFC contact, and in most cases, Permian phyllites and light schist underlay Carboniferous schists or large-scale Carboniferous/Permian-Triassic schist or phyllite packages that appear in sheets (Figures 7A,F). These old on top of young relationships show evidence for discrete thrust faults within Alpujárride and close to the contact with the NFC along the major detachment fault. None of these thrust faults are crosscutting the low-angle normal fault and offsetting lithologies within the NFC; hence their movements must be prior to the juxtaposition of the two complexes. Thrust faults and nappe stacking in Alpujárride have been previously

identified by various studies (e.g., Booth-Rea et al., 2002; Rossetti et al., 2005; Simancas, 2018) although the timing of their formation is debated. Booth-Rea et al. (2002) and Simancas, (2018) attribute this thrusting to a post-metamorphic event prior to extension. In contrast, Rossetti et al. (2005) support that these thrust nappes are related to a compressional ductile deformation event during Cenozoic subduction. Although our new data sets robust constraints on these thrusts on the basis of age reversals from densely spaced samples, additional work is needed to establish the precise timing of these events and is the central topic of a future study. Following the formation of thrust nappes, the Alpujárride units experienced extensional processes related to the Late Miocene extension that brought the Alpujárride complex to its current configuration (Rossetti et al., 2005).

There are eight main zircon age modes observed in the Alpujárride Complex, including Permian (251–298 Ma), Carboniferous (298–358 Ma), Early Paleozoic (358–541 Ma), Ediacaran (541–635 Ma), Early Neoproterozoic (635–1,000 Ma), Mesoproterozoic (1,000–1,600 Ma), Paleoproterozoic (1,600–2,500 Ma), and Archean (>2,500 Ma) (Figure 8; see Supplementary Table S1 for statistics). Multidimensional Scaling Plots show the similarity between the NFC and Alpujárride units (Figure 6) and enhance the recently published data from Jabaloy-Sánchez et al. (2021) that showed similar patterns in Carboniferous and Permian zircon sources between both units. Our updated compilation shows that the DZ spectra between NFC and Alpujárride are remarkably similar (Figure 6C). Additionally, previous work on the orthogneisses from the Alpujárride also yielded Permian ages, indicating coeval granitoid emplacement to those within the NFC (Zeck & Whitehouse, 1999; García-Casco et al., 2014). Our data support previous work by Jabaloy-Sánchez et al. (2018), Jabaloy-Sánchez et al. (2021) demonstrated the similarity of the Carboniferous strata in NFC and Alpujárride with the Cantabrian Zone (Pastor-Galan et al., 2013) and the dissimilarities among other zones of the Iberia Massif, South Portuguese Zone (Pereira et al., 2014), and Ossa-Morena zone (Dinis et al., 2018; Pereira et al., 2020). Since the focus of this study is on the Central/East part of Alpujárride outcrops near the contact with the NFC, we only collected samples from Paleozoic strata (Permian and older) and our dataset does not contain Triassic strata that record rifting. However, there is robust evidence in the carbonate platform of the Sierra de la Contraviesa that this region has experienced rifting in the Middle/Late Triassic due to the presence of normal faults and syn-kinematic deposition characteristics (Martín-Rojas et al., 2009, 2012).

4.5 Correlations of the Nevado-Filábride Complex with Alpujárride in the Paleozoic

Deposition of the NFC began in the Devonian and continued into the Early Jurassic, which is a crucial timespan shaping tectonics of the Western Mediterranean realm (Figure 8). Here,

new detailed geochronologic constraints provide key data and observations to better understand the paleogeographic evolution of the region and its relationship with the Alpujárride Complex in the Internal Betics. There have been only four samples analyzed from the Maláguide complex (Esteban et al., 2017; Jabaloy-Sánchez et al., 2021) and from internal zones of the Rif Cordillera (Azdimousa et al., 2019); hence a robust correlation between all internal units is not possible at this time. We compare our provenance results with a recent DZ compilation by Stephan et al. (2019) to decipher unique source terranes, including Avalonia, West Africa, East Africa-Arabia, and Baltica/Peri-Laurentia. Provenance signals from subduction complexes in this compilation are poorly constrained or entirely missing. We plotted our DZ spectra from 800 to 3,500 Ma for both the NFC and Alpujárride (Figure 9C) and compared these to the provenance compilation from Stephan et al. (2019). The DZ spectra of NFC and Alpujárride are dominated by Northeast Africa sources, similar to rocks along the majority of the central and eastern Iberian Peninsula. The main characteristics of this Northeastern Africa margin spectra are pronounced zircon age peaks sourcing the Grenvillian orogeny and the absence of zircon sources from 1,200 to 1700 Ma, along with a flat distribution of ages from 1700 to 2,800 Ma (Figure 9C).

The Carboniferous Veleta unit of the NFC represents the basement sequence that was involved in the Variscan orogeny and contains similar sources to the Carboniferous strata of the Alpujárride complex (Figure 9A). These ages agree with data obtained by conodonts in the Bodurria unit (NFC) in west Sierra de los Filabres (Sierra de Baza; Rodríguez-Cañero et al., 2018). Additionally, the recent provenance study from Jabaloy-Sánchez et al. (2021) comparing the two complexes shows that the NFC and Alpujárride have similar zircon age modes in Carboniferous and Permian in the Aguilas Arc as well as similar zircon sources with the Cantabrian zone in Iberia (Pastor-Galán et al., 2013). The same data compilation shows the dissimilarity of the NFC with samples collected from the NE Iberia Peninsula, South France, and Ossa Morena (Dinis et al., 2018; Pereira et al., 2020). In this study, our extensive dataset from the NFC and the Alpujárride complex and the MDS plots generated comparing the two based on their MDAs strongly support the recently published data and indicate that the two complexes were deposited nearby and received the same sedimentary sources (Figures 6C,9A,9B).

During the Early Permian, felsic magmatism is found in both the NFC (this study; Gómez-Pugnaire et al., 2012) and Alpujárride (Zeck & Whitehouse, 1999; Sánchez-Navas et al., 2014) (Figure 9B). Permian magmatism is observed in the North Atlantic (Angrand et al., 2020) and Western Europe (Soto et al., 2017) including the Iberian peninsula (Lago et al., 2005; Denèle et al., 2012; Lopez-Gomez et al., 2019). Contrary to previous observations, we find orthogneisses within the Mulhacén succession and they are entirely absent from the Veleta unit. This indicates that granitoids preferentially

intruded into the overlaying Mulhacén succession. Since this succession is more heterogeneous and has evidence of basic lithologies, one explanation is that the Mulhacén succession was largely deposited in a more distal domain associated with rifting, whereas Veleta was proximal to orogenic uplifts from the Variscan orogeny (Figure 10).

4.6 Early Mesozoic tectonic evolution of the Nevado-Filábride Complex and Alpujárride

The Triassic/Jurassic period is critical in the Mediterranean, with rifting occurring in different segments, including the Western Alps (Megard-Galli & Faure, 1988), the Southern Alps (Bertotti et al., 1993), and Iberia (Sopeña et al., 1988). This timing is particularly important since it marks the beginning of the Alpine cycle and geochronometric constraints can help distinguish numerous differing plate tectonic reconstructions (Arche & López-Gómez, 1996; Baudon et al., 2009; De Vicente and Vegas, 2009; McKie and Williams, 2009; Perri et al., 2013). Evidence from the Western Mediterranean is sparse during this time since Iberia may have been an isolated microplate and much of the geologic record was destroyed in subsequent subduction/ collision events (e.g., Rosenbaum et al., 2002). The magmatic expression of rifting in the Western Mediterranean includes the Central Atlantic Magmatic Province (CAMP) event which emplaced dykes and basaltic magmatism (Azambre et al., 1987). Widespread deposition of evaporites was also prevalent at this time (Angrand and Mouthereau, 2021). The record of rifting in the Internal Betics was previously noted based on the presence of metabasites (Puga et al., 2017) and preserved syn-rift structures (Martín-Rojas et al., 2009); however, this is the first study to report provenance data on Triassic Alpujárride strata and Triassic-Early Jurassic NFC strata.

In the NFC, the metabasitic rocks have yielded zircon ages and Rb-Sr isochron of ~185–146 Ma (Hebeda et al., 1980; Bodinier et al., 1987; Puga et al., 2005, 2011, 2017). We report the first data from Early Jurassic metabasitic dykes in the Veleta unit (Figures 6, 9C), while in the Alpujárride complex, continued Triassic rifting is recorded by syn-kinematic extensional structures in Triassic strata (Martín-Rojas et al., 2009) and the presence of gabbroic rocks at ~180 Ma (Tubía et al., 2009). Similarly, in the Rif Cordillera, a range of 195–200 Ma zircon ages from gabbroid samples from the Beni-Malek peridotite are interpreted as the continuation of rifting (Gimeno-Vives et al., 2019). Ultramafic rocks in the external Rif Cordillera have been previously dated at 166 Ma (Michard et al., 1992; Benzaggagh et al., 2014). Zircon rims with Jurassic and Early Cretaceous ages have also been found in the Jubrique Unit in pyroxenites (Sánchez-Rodríguez & Gebauer, 2000), suggesting that some exhumation either of the mantle or the lower crustal rocks was accommodated by the late stages of rifting. In this study, apatite U-Pb ages indicate that metabasites in the lower Veleta unit

are 197 Myrs old (Figures 6, 10C). These ages are widespread in the Western Mediterranean and related to the CAMP event (Marzoli et al., 2018). The formation of a new oceanic crust separating Africa from Iberia (Michard et al., 1992; Durand-Delga et al., 2000; Puga et al., 2011; van Hinsbergen et al., 2014) as a western segment of the Ligurian Neo-Tethys Ocean was coeval with emplacement of these metabasitic dykes.

The two generations of ages in the Late Triassic/Early Jurassic and Late Jurassic can be correlated with distinct pulses of accelerated rifting that initiated in the Triassic and continued into the Jurassic. These stages of rifting have been identified in other parts of the Iberian plate (Asti et al., 2019; Pedrera et al., 2020). Our results support that the Veleta unit records sedimentary fluxes during Variscan orogenesis and later acted as a proximal basement suite during extension and the intrusion of CAMP dykes, while the overlying Mulhacén succession solely records Permian–Jurassic post-Variscan extension and rifting (Puga et al., 2005). The deposition of the Triassic metadetrital Tahal formation and the deposition of evaporite deposits elsewhere in Iberia at this time reflect the late stages of rifting in the Western Mediterranean and support the proximity of NFC with the Iberian margin. Our new constraints with Triassic–Jurassic ages in the NFC that record regional rifting will enhance future paleogeographic reconstructions of the Mediterranean since age constraints are sparse during this time (Angrand and Mouthereau, 2021). Following a second pulse of rifting in the Late Jurassic, we found an absence of zircon sources in both units. This could suggest that rifting was complete at this time and no new zircon sources were established, or a transition to dominantly chemical sedimentation was evident by the carbonate platforms in both units. Even though more investigation is needed for the exact position of the Maláguide, based on the recent work by Jabaloy-Sánchez et al. (2021), the complex would be positioned eastward of Alpujarride and separated by Iberia already by Jurassic.

4.7 Implications for the tectonic evolution of the western Mediterranean

The tectonic affinity of the NFC and Alpujárride and its relationship to the Iberian and African margins remains debated. The first studies published for the Betic Cordillera argued that all the internal units were originally part of the Alboran domain of the AlKaPeCa block (Lonergan & Platt, 1995). More recent studies have revisited the origins of the NFC and suggested it was formed along the southern Iberian margin (e.g., Platt et al., 2006; Kirchner et al., 2016), while Alpujárride represented a more distal terrane in the Alboran domain (e.g., Tubía et al., 2009). This scenario was attributed mostly to the different timings and grades of metamorphism between the two units. These differences in metamorphic nature, as well as the stacking of the initially separated NFC and Alpujárride, were explained by subduction of the NFC to the south underneath the Alpujárride

Complex. However, this hypothesis has been challenged after recent studies have revealed that the two units have similar peak metamorphic ages during the Eocene (Augier et al., 2005b; Li and Massonne, 2018; Poulaki et al., 2020; Bessière et al., 2021a, Bessière et al., 2021b; Aerden et al., 2020). Based on our provenance data showing similar sedimentary sources throughout their depositional history, we suggest that the NFC and Alpujárride originated and remained in proximity to each other. Paleozoic strata in both units have remarkably similar age modes with the Cantabrian zone of the Iberian Massif, agreeing with recently published data from Jabaloy-Sánchez et al. (2021) that they were deposited along the southern Iberian margin throughout this period. Furthermore, the proximity of NFC to Alpujárride is supported by similar composition and timing of granitoid emplacement in the Permian, Triassic–Jurassic carbonate sequences, and Early Jurassic metabasites. We argue that the NFC and Alpujárride reflect similar stratigraphic successions throughout the Paleozoic and that the primary variations can be attributed to changing Mesozoic deposition environments during the final stages of rifting and different metamorphic histories from Cenozoic subduction and exhumation.

The tectonic configuration of the region in the Jurassic is essential for understanding the onset of the subduction in the Cenozoic and hence convergence between Africa and Iberia. The rift configuration of the NFC has also been recently imaged by using receiver function tomography and has identified the proximal and necking domains of the NFC below southern Iberia (Morales et al., 2022) and has been proposed to be a magma-poor rifted margin, which could explain the very few to absent zircon sources during this time. It is possible that the NFC and Alpujárride were laterally equivalent to each other but NFC in deeper water due to more extension during the rift phase, while Alpujárride rests on a more buoyant block (Figure 10D). Eocene HP/LT metamorphic ages have been reported for both Alpujárride and the NFC (Monié et al., 1991; Augier et al., 2005a; Platt et al., 2005; Li and Massonne, 2018; Aerden et al., 2020; Bessière et al., 2021b), which indicates that the units were subducted at similar times with the NFC experiencing HP metamorphism up to 18–22 kbar (e.g., Gómez-Pugnaire and Franz, 1988; Augier et al., 2005a; Li and Massonne, 2018; Santamaría-López et al., 2019) but Alpujárride to smaller depths of around 13–15 kbar (Tubía & Ibarguchi, 1991; García-Casco and Torres Roldán, 1999; Azañón & Crespo-Blanc, 2000). It is also generally accepted that the Alpujárride complex has been exhumed prior to the NFC with the presence of low-angle normal faults and Alpujárride overlaying the NFC representing the upper plate (e.g., Sánchez-Vizcaíno et al., 2001; Augier et al., 2005a). These lines of evidence indicate that the subduction is at similar times with Alpujárride entering the subduction system first and the NFC following laterally adjacent to it.

Hence, the question remains whether the NFC and Alpujárride rifted away from Iberia during Triassic–Jurassic,

or if they remained proximal and represented the southern Iberian passive margin sequence up until Cenozoic convergence. In the first scenario, both Alpujárride and NFC are close to southern Iberia in the Late Jurassic, but potentially separated by a small oceanic basic or hyperextended continental domain. The proposed existence of a narrow oceanic basic separating Iberia from NFC/Alpujárride is based on evidence for the subsequent incorporation of ultramafic/mafic rocks into the Internal Betics and the necessity for a zone of weakness to initiate a north-dipping subduction zone in the Cenozoic. This narrow oceanic domain may have been a branch of the Ligurian Tethys involving oceanic crust and hyperextended continental crust with exhumed mantle peridotite, as proposed by earlier studies (Bessière et al., 2021a). These alternative scenarios have important implications for the polarity of subduction and convergence during the Cenozoic. If the NFC and Alpujárride represent the rifted margin of southern Iberia (Rehault et al., 1984; Frizon de Lamotte et al., 2000; Behr & Platt, 2013), they must have been subducted together toward the south since the close timing of subduction metamorphism between the units is undisputed. However, the lack of sources from the Jurassic to the Cenozoic, which are present in the external zones and show clear affinity with the southern Iberian margin, makes this scenario less plausible. Additionally, this scenario requires either the presence of a two-sided subduction zone or a subduction polarity reversal, both of which are controversial and have limited geologic evidence and geodynamic models supporting them (Chertova et al., 2014).

Alternatively, in the scenario that the NFC and Alpujárride rifted away, a separate Betic ocean or the hyperextended continental domain must have existed between NFC/Alpujárride and southern Iberia. This arrangement would involve the initiation of a new subduction zone near the southern Iberian margin with north-dipping polarity to subsequently close the narrow ocean (Figure 10D). In that case, the NFC and Alpujárride could have been subducted and accreted back onto the Iberian margin, with mafic/ultramafic lithologies representing remnants of the oceanic domain that existed between them and involved in the obduction process. A sole north-dipping slab is supported by many previous studies (Rosenbaum et al., 2002; Faccenna et al., 2004; Booth-Rea et al., 2007; Bezada et al., 2013; Chertova et al., 2014). Furthermore, external zones of the Betic Cordillera represent unmetamorphosed southern Iberian passive margin sequences, and the internal zones are highly metamorphosed and thrusted onto them. These relationships are best explained by the initial separation of NFC/Alpujárride with Iberia and a north-dipping slab so that the NFC/Alpujárride could be subducted together and emplaced back onto the Iberian crust.

We propose that the NFC and Alpujárride were deposited proximal to the southern Iberian margin throughout the Paleozoic but were separated by Mesozoic rifting processes. A narrow wedge-shaped oceanic basin opened at this time, with

Alpujárride situated closer to Iberia atop the less-thinned crust, while NFC lies southwest of Alpujárride in a more thinned zone with a wider swatch of the oceanic crust in the new Betic ocean (Figure 10B). The opening of the North and South Atlantic during the Cretaceous and Early Cenozoic caused a change in plate motions and led to the northwest movement of Africa. Convergence was accommodated by the initiation of a north-dipping subduction zone, potentially along the weak continent-ocean transition of the magma-poor southern Iberian margin. Due to the wedge-shaped Betic ocean and plate rotation, Alpujárride was subducted first beneath the southern Iberian margin, followed by subduction of the laterally adjacent NFC as the system propagated to the west. The existence of a wider oceanic domain between the NFC and Iberia in comparison to Alpujárride, in combination with thinner crust resulting in a denser lithosphere, may have provided increased slab pull forces to drive subduction and could explain why the NFC was subducted deeper than Alpujárride which shows a lesser degree of subduction metamorphism. The warm and highly coupled earlier stages of subduction may have allowed for underplating and capture of NFC and Alpujárride onto the Iberian margin in the overriding plate. Subsequent closure of the Maghrebian ocean along the same north-dipping subduction zone involved rapid slab roll back, extension in the overriding plate, and translation of the Alboran domain to its present-day position. The switch to extension in the overriding plate in the Late Miocene allowed for the exhumation of the NFC and Alpujárride into their current architecture in the Betic Cordillera.

5 Conclusion

Our detailed stratigraphic framework with new zircon and apatite U-Pb depth profile and petrographic observations from the NFC and Eastern Alpujárride provide key constraints on the complicated paleogeographic evolution of the Western Mediterranean. We found that the NFC has maximum depositional ages that range from Devonian to Triassic/Early Jurassic. The sequence records long-lived deposition from the Variscan orogeny to the opening of the Alpine Tethys and completes the Wilson cycle with subduction in Cenozoic but with a notable hiatus in ages from Jurassic to subduction initiation. The provenance within the NFC subunits does not change throughout its lifetime with the only differences representing the youngest age mode that also defines the MDA. The presence of 197 Ma metabasites within the lowest Carboniferous Veleta unit shows that it acted as a basement and experienced extension and the intrusion of CAMP dykes during the opening of the Central Atlantic. The Mulhacén succession is more heterogeneous including lithologies from Early Permian to Early Jurassic. During this time, the overlying Mulhacén

succession records sedimentary fluxes with the presence of Triassic and Early Jurassic metasedimentary rocks.

Evidence of rifting in Alpujárride includes the presence of metabasites as well as syn-rift structures in the Triassic strata documented elsewhere. Comparison between the zircon data from Alpujárride and NFC shows similar provenance sources from Carboniferous to Permian and match the signatures of Central Iberia. Based on these similarities, we propose that the units are depositing in the same or close by basins near the Southern Iberia margin and are not allochthonous terranes as previously suggested. Integrating our results with previous findings, we propose an updated paleogeographic model where a narrow wedge-shaped oceanic basin opened at this time and separated the NFC and Alpujárride from the Iberia margin and followed by a north-dipping subduction zone. Our new framework reconciles earlier controversies about the structures and ages of the NFC and Alpujárride, their relationship to Southern Iberia, and tectonic configurations prior to Cenozoic convergence and subduction in the Western Mediterranean.

Data availability statement

The datasets presented in this study can be found in online repositories. The names of the repository/repositories and accession number(s) can be found in the article/Supplementary Material. Data can also be found online at geochron.org

Author contributions

EP and DS contributed to the conception and design of the study. Both authors went to the field. EP collected and analyzed the data and wrote the first draft of the manuscript. Both authors contributed to the manuscript revision and approved the final submitted version.

Funding

Acknowledgments

assistance in the UT Chron laboratories and Phil Orlandini for the collection and processing of the EDS maps. They thank Sofia Laskari for her assistance in the first field season, as well as Claudio Faccenna, and Mark Cloos, for insightful discussions. The authors would also like to thank Guillermo Booth-Rea for the editorial handling of the manuscript and Antonio Jabaloy Sánchez and Azdimousa Ali for the constructive feedback that greatly improved the manuscript.

Conflict of interest

The authors declare that the research was conducted in the absence of any commercial or financial relationships that could be construed as a potential conflict of interest.

Publisher's note

All claims expressed in this article are solely those of the authors and do not necessarily represent those of their affiliated organizations, or those of the publisher, the editors, and the reviewers. Any product that may be evaluated in this article, or claim that may be made by its manufacturer, is not guaranteed or endorsed by the publisher.

Supplementary material

The Supplementary Material for this article can be found online at: https://www.frontiersin.org/articles/10.3389/feart.2022.929502/full#supplementary-material

References

Accotto, C., Poyatos, D. M., Azor, A., Talavera, C., Evans, N. J., Jabaloy–Sánchez, A., et al. (2021). Systematics of detrital zircon U–Pb ages from Cambrian–Lower Devonian rocks of northern Morocco with implications for the northern Gondwanan passive margin. *Precambrian Res.* 365, 106366. doi:10.1016/j.precamres.2021.106366

Aerden, D., Farrell, T. P., Baxter, E., Stewart, E., and Bouybaouene, M. L. (2020). *Tectonic evolution of the Betic-Rif orogen constrained by 3-D microstructural analysis and Sm-Nd dating of garnet porphyroblasts.*

Aguado, B. V., Azevedo, M. R., Schaltegger, U., Catalán, J. M., and Nolan, J. (2005). U–Pb zircon and monazite geochronology of Variscan magmatism related to syn-convergence extension in Central Northern Portugal. *Lithos* 82 (1-2), 169–184. doi:10.1016/j.lithos.2004.12.012

Alonso-Chaves, F. M., and Orozco, M. (2007). Evolución tectónica de las Sierras de Tejeda y Almijara: Colapso extensional y exhumación de áreas metamórficas en el dominio de Alborán (Cordilleras Béticas). *Rev. Soc. Geol. España* 20 (3-4), 211–228.

Andrieux, J., Frizon de Lamotie, D., and Braud, J. (1989). A structural scheme for the Western Mediterranean area in Jurassic and Early Cretaceous times. *Geodin. Acta* 3 (1), 5–15. doi:10.1080/09853111.1989.11105171

Angrand, P., and Mouthereau, F. (2021). Evolution of the Alpine orogenic belts in the Western Mediterranean region as resolved by the kinematics of the Europe-Africa diffuse plate boundary. *BSGF - Earth Sci. Bull.* 192 (1), 42. doi:10.1051/bsgf/2021031

Angrand, P., Mouthereau, F., Masini, E., and Asti, R. (2020). A reconstruction of Iberia accounting for western Tethys–North Atlantic kinematics since the late-permian–triassic. *Solid earth.* 11 (4), 1313–1332. doi:10.5194/se-11-1313-2020

Arche, A., and López-Gómez, J. (1996). Origin of the permian-triassic Iberian basin, central-eastern Spain. *Tectonophysics* 266 (1-4), 443–464. doi:10.1016/s0040-1951(96)00202-8

Asti, R., Lagabrielle, Y., Fourcade, S., Corre, B., and Monié, P. (2019). How do continents deform during mantle exhumation? Insights from the northern Iberia inverted paleopassive margin, Western pyrenees (France). *Tectonics* 38 (5), 1666–1693. doi:10.1029/2018tc005428

Augier, R., Agard, P., Monié, P., Jolivet, L., Robin, C., Booth-Rea, G., et al. (2005). Exhumation, doming and slab retreat in the betic cordillera (SE Spain): *In situ* 40Ar/39Ar ages and P–T–d–t paths for the nevado-filabride complex. *J. Metamorph. Geol.* 23 (5), 357–381. doi:10.1111/j.1525-1314.2005.00581.x

Augier, R., Jolivet, L., and Robin, C. (2005). Late Orogenic doming in the eastern Betic Cordilleras: Final exhumation of the Nevado-Filabride complex and its relation to basin Genesis. *Tectonics* 24 (4). doi:10.1029/2004tc001687

Azambre, B., Rossy, M., and Lago, M. (1987). Caracteristiques petrologiques des dolerites tholeiitiques d'age triasique (ophites) du domaine pyreneen. *bulmi.* 110 (4), 379–396. doi:10.3406/bulmi.1987.8035

Azañón, J. M., and Crespo-Blanc, A. (2000). Exhumation during a continental collision inferred from the tectonometamorphic evolution of the Alpujárride Complex in the central Betics (Alboran Domain, SE Spain). *Tectonics* 19 (3), 549–565. doi:10.1029/2000tc900005

Azanon, J. M., Garcia-Due as, V., Martinez-Martinez, J. M., and Crespoblanc, A. (1994). Alpujárride tectonic sheets in the central Betics and similar eastern allochthonous units (SE Spain). *C. R. Acad. Sci. PARIS* 318, 667.

Azañón, J. M., and Goffé, B. (1997). Ferro- and magnesiocarpholite assemblages as record of high-P, low-Γ metamorphism in the Central Alpujarrides, Betic Cordillera (SE Spain). *Eur. J. Mineral.* 9, 1035–1052. doi:10.1127/ejm/9/5/1035

Azdimousa, A., Jabaloy-Sánchez, A., Talavera, C., Asebriy, L., González-Lodeiro, F., Evans, N. J., et al. (2019). Detrital zircon U-Pb ages in the Rif Belt (northern Morocco): Paleogeographic implications. *Gondwana Res.* 70, 133–150. doi:10.1016/j.gr.2018.12.008

Balanyá, J. C., Campos, J., García Dueñas, V., Orozco, M., and Simancas Cabrera, J. F. (1987). *Generaciones de cabalgamientos y pliegues recumbentes en los Mantos Alpujárrides entre Ronda y Almería, Cordilleras Béticas.* Madrid, Spain: Sociedad Geológica de España.

Barnett-Moore, N., Hosseinpour, M., and Maus, S. (2016). Assessing discrepancies between previous plate kinematic models of Mesozoic Iberia and their constraints. *Tectonics* 35 (8), 1843–1862. doi:10.1002/2015tc004019

Baudon, C., Fabuel-Perez, I., and Redfern, J. (2009). Structural style and evolution of a late Triassic rift basin in the central high atlas, Morocco: Controls on sediment deposition. *Geol. J.* 44 (6), 677–691. doi:10.1002/gj.1195

Bea, F., Montero, P. G., Gonzalez-Lodeiro, F., Talavera, C., Molina, J. F., Scarrow, J. H., et al. (2006). Zircon thermometry and U–Pb ion-microprobe dating of the gabbros and associated migmatitesof the variscan toledo anatectic complex, central Iberia. *J. Geol. Soc.* 163 (5), 847–855. doi:10.1144/0016-76492005-143

Bea, F., Montero, P., González-Lodeiro, F., and Talavera, C. (2007). Zircon inheritance reveals exceptionally fast crustal magma generation processes in Central Iberia during the Cambro-Ordovician. *J. petrology* 48 (12), 2327–2339. doi:10.1093/petrology/egm061

Bea, F., Montero, P., Talavera, C., Abu Anbar, M., Scarrow, J. H., Molina, J. F., et al. (2010). The palaeogeographic position of central Iberia in Gondwana during the ordovician: Evidence from zircon chronology and Nd isotopes. *Terra nova.* 22 (5), 341–346. doi:10.1111/j.1365-3121.2010.00957.x

Behr, W. M., and Platt, J. P. (2012). Kinematic and thermal evolution during two-stage exhumation of a Mediterranean subduction complex. *Tectonics* 31 (4). doi:10.1029/2012tc003121

Behr, W. M., and Platt, J. P. (2013). Rheological evolution of a Mediterranean subduction complex. *J. Struct. Geol.* 54, 136–155. doi:10.1016/j.jsg.2013.07.012

Benzaggagh, M., Mokhtari, A., Rossi, P., Michard, A., El Maz, A., Chalouan, A., et al. (2014). Oceanic units in the core of the external Rif (Morocco): Intramargin hiatus or south-tethyan remnants? *J. Geodyn.* 77, 4–21. doi:10.1016/j.jog.2013.10.003

Bertotti, G., Picotti, V., Bernoulli, D., and Castellarin, A. (1993). From rifting to drifting: Tectonic evolution of the south-alpine upper crust from the triassic to the early cretaceous. *Sediment. Geol.* 86 (1-2), 53–76. doi:10.1016/0037-0738(93)90133-p

Bessière, E., Augier, R., Jolivet, L., Précigout, J., and Romagny, A. (2021). Exhumation of the ronda peridotite during hyper-extension: New structural and thermal constraints from the nieves unit (Western betic cordillera, Spain). *Tectonics* 40 (10), e2020TC006271. doi:10.1029/2020tc006271

Bessière, E., Jolivet, L., Augier, R., Scaillet, S., Précigout, J., Azañon, J. M., et al. (2021). Lateral variations of pressure-temperature evolution in non-cylindrical orogens and 3-D subduction dynamics: The betic-rif cordillera example. *BSGF - Earth Sci. Bull.* 192 (1), 8. doi:10.1051/bsgf/2021007

Bezada, M. J., Humphreys, E. D., Toomey, D. R., Harnafi, M., Dávila, J. M., Gallart, J., et al. (2013). Evidence for slab rollback in westernmost Mediterranean from improved upper mantle imaging. *Earth Planet. Sci. Lett.* 368, 51–60. doi:10.1016/j.epsl.2013.02.024

Biari, Y., Klingelhoefer, F., Sahabi, M., Funck, T., Benabdellouahed, M., Schnabel, M., et al. (2017). Opening of the central Atlantic Ocean: Implications for geometric rifting and asymmetric initial seafloor spreading after continental breakup. *Tectonics* 36 (6), 1129–1150. doi:10.1002/2017tc004596

Bodinier, J. L., Morten, L., Puga, E., and de Federico, A. D. (1987). Geochemistry of metabasites from the nevado-filabride complex, betic cordilleras, Spain: Relics of a dismembered ophiolitic sequence. *Lithos* 20 (3), 235–245. doi:10.1016/0024-4937(87)90011-9

Booth-Rea, G., Azañón, J. M., Goffé, B., Vidal, O., and Martı́nez-Martı́nez, J. M. (2002). High-pressure, low-temperature metamorphism in Alpujárride units of southeastern Betics (Spain). *Comptes Rendus Geosci.* 334 (11), 857–865. doi:10.1016/s1631-0713(02)01787-x

Booth-Rea, G., Ranero, C. R., Martínez-Martínez, J. M., and Grevemeyer, I. (2007). Crustal types and Tertiary tectonic evolution of the Alborán sea, Western Mediterranean. *Geochem. Geophys. Geosyst.* 8 (10). doi:10.1029/2007gc001639

Bouillin, J. P., Durand-Delga, M., and Olivier, P. (1986). Betic-rifian and tyrrhenian arcs: Distinctive features, Genesis and development stages. *Dev. Geotect.* 21, 281–304. doi:10.1016/B978-0-444-42688-8.50017-5

Brun, J. P., and Faccenna, C. (2008). Exhumation of high-pressure rocks driven by slab rollback. *Earth Planet. Sci. Lett.* 272 (1-2), 1–7. doi:10.1016/j.epsl.2008.02.038

Calvert, A., Sandvol, E., Seber, D., Barazangi, M., Roecker, S., Mourabit, T., et al. (2000). Geodynamic evolution of the lithosphere and upper mantle beneath the Alboran region of the Western Mediterranean: Constraints from travel time tomography. *J. Geophys. Res.* 105 (B5), 10871–10898. doi:10.1029/2000jb900024

Cambeses, A., Scarrow, J. H., Montero, P., Molina, J. F., and Moreno, J. A. (2015). SHRIMP U–Pb zircon dating of the Valencia del Ventoso plutonic complex, Ossa-Morena Zone, SW Iberia: Early Carboniferous intra-orogenic extension-related 'calc-alkaline'magmatism. *Gondwana Res.* 28 (2), 735–756. doi:10.1016/j.gr.2014.05.013

Campos-Soto, S., Benito, M. I., Cobos, A., Caus, E., Quijada, I. E., Suarez-Gonzalez, P., et al. (2019). Revisiting the age and palaeoenvironments of the upper jurassic–lower cretaceous? Dinosaur-bearing sedimentary record of eastern Spain: Implications for iberian palaeogeography. *J. Iber. Geol.* 45 (3), 471–510. doi:10.1007/s41513-019-00106-y

Carminati, E., Lustrino, M., and Doglioni, C. (2012). Geodynamic evolution of the central and Western Mediterranean: Tectonics vs. igneous petrology constraints. *Tectonophysics* 579, 173–192. doi:10.1016/j.tecto.2012.01.026

Carminati, E., Wortel, M. J. R., Meijer, P. T., and Sabadini, R. (1998). The two-stage opening of the Western–central mediterranean basins: A forward modeling test to a new evolutionary model. *Earth Planet. Sci. Lett.* 160 (3-4), 667–679. doi:10.1016/s0012-821x(98)00119-8

Chalouan, A., Michard, A., Kadiri, K., Negro, F., Lamotte, D., Soto, J. I., et al. (2008). "The Rif belt," in *Continental evolution: The geology of Morocco* (Berlin, Heidelberg: Springer), 203–302.

Chertova, M. V., Spakman, W., Geenen, T., Van Den Berg, A. P., and Van Hinsbergen, D. J. J. (2014). Underpinning tectonic reconstructions of the Western Mediterranean region with dynamic slab evolution from 3-D numerical modeling. *J. Geophys. Res. Solid Earth* 119 (7), 5876–5902. doi:10.1002/2014jb011150

Csontos, L., and Vörös, A. (2004). Mesozoic plate tectonic reconstruction of the Carpathian region. *Palaeogeogr. Palaeoclimatol. Palaeoecol.* 210 (1), 1–56. doi:10.1016/j.palaeo.2004.02.033

de Saint Blanquat, M. (1993). La faille normale ductile du massif du Saint Barthélémy. Evolution hercynienne des massifs nord-pyrénéens catazonaux considérée du point de vue de leur histoire thermique. *Geodin. Acta* 6 (1), 59–77. doi:10.1080/09853111.1993.11105239

de Saint Blanquat, M., Lardeaux, J. M., and Brunel, M. (1990). Petrological arguments for high-temperature extensional deformation in the pyrenean variscan crust (Saint barthélémy massif, ariège, France). *Tectonophysics* 177 (1-3), 245–262. doi:10.1016/0040-1951(90)90284-f

De Vicente, G., and Vegas, R. (2009). Large-scale distributed deformation controlled topography along the Western Africa–Eurasia limit: Tectonic constraints. *Tectonophysics* 474 (1-2), 124–143. doi:10.1016/j.tecto.2008.11.026

Delgado, F., Estévez, A., Martín, J. M., and Martín-Algarra, A. (1981). *Estud. Geol.* 37, 45–57.

Denèle, Y., Paquette, J. L., Olivier, P., and Barbey, P. (2012). Permian granites in the pyrenees: The aya pluton (Basque country). *Terra nova.* 24 (2), 105–113. doi:10.1111/j.1365-3121.2011.01043.x

Deptuck, M. E., and Kendell, K. L. (2017). "A review of Mesozoic-Cenozoic salt tectonics along the Scotian margin, eastern Canada," in *Permo-triassic salt provinces of Europe, north Africa and the atlantic margins* (Amsterdam, Netherlands: Elsevier), 287–312.

Dercourt, J., Zonenshain, L. P., Ricou, L. E., Kazmin, V. G., Le Pichon, X., Knipper, A. L., et al. (1986). Geological evolution of the Tethys belt from the atlantic to the pamirs since the lias. *Tectonophysics* 123 (1-4), 241–315. doi:10.1016/0040-1951(86)90199-x

Dewey, J. F., Helman, M. L., Knott, S. D., Turco, E., and Hutton, D. H. W. (1989). Kinematics of the Western mediterranean. *Geol. Soc. Lond. Spec. Publ.* 45 (1), 265–283. doi:10.1144/gsl.sp.1989.045.01.15

Dinis, P. A., Fernandes, P., Jorge, R. C., Rodrigues, B., Chew, D. M., Tassinari, C. G., et al. (2018). The transition from Pangea amalgamation to fragmentation: Constraints from detrital zircon geochronology on West Iberia paleogeography and sediment sources. *Sediment. Geol.* 375, 172–187. doi:10.1016/j.sedgeo.2017.09.015

Durand-Delga, M., Rossi, P., Olivier, P., and Puglisi, D. (2000). Situation structurale et nature ophiolitique de roches basiques jurassiques associées aux flyschs maghrébins du Rif (Maroc) et de Sicile (Italie). *Comptes Rendus de l'Academie. des Sci. - Ser. IIA - Earth Planet. Sci.* 331 (1), 29–38. doi:10.1016/s1251-8050(00)01378-1

Esteban, J. J., Cuevas, J., Tubía, J. M., Gutiérrez-Alonso, G., Larionov, A., Sergeev, S., et al. (2017). U–Pb detrital zircon ages from the paleozoic marbella conglomerate of the malaguide complex (betic cordilleras, Spain). Implications on paleotethyan evolution. *Lithos* 290, 34–47. doi:10.1016/j.lithos.2017.07.022

Esteban, J. J., Cuevas, J., and Tubía, J. M. (2022). Peri-gondwanan provenance and geodynamic evolution of the guadaiza nappe (Alpujarride complex, betic cordilleras, Spain): Insights on the paleotethyan paleogeography. *Minerals* 12 (3), 325. doi:10.3390/min12030325

Faccenna, C., Piromallo, C., Crespo-Blanc, A., Jolivet, L., and Rossetti, F. (2004). Lateral slab deformation and the origin of the Western Mediterranean arcs. *Tectonics* 23 (1). doi:10.1029/2002tc001488

Favre, P., and Stampfli, G. M. (1992). From rifting to passive margin: The examples of the red sea, central atlantic and alpine Tethys. *Tectonophysics* 215 (1-2), 69–97. doi:10.1016/0040-1951(92)90075-h

Fernández, R. D., Pereira, M. F., and Foster, D. A. (2015). Peralkaline and alkaline magmatism of the Ossa-Morena zone (SW Iberia): Age, source, and implications for the Paleozoic evolution of Gondwanan lithosphere. *Lithosphere* 7 (1), 73–90. doi:10.1130/l379.1

Fernández-Suárez, J., Gutiérrez-Alonso, G., Jenner, G. A., and Tubrett, M. N. (2000). New ideas on the proterozoic-early palaeozoic evolution of NW Iberia: Insights from U–Pb detrital zircon ages. *Precambrian Res.* 102 (3-4), 185–206. doi:10.1016/s0301-9268(00)00065-6

Fernández-Suárez, J., Gutierrez-Alonso, G., Johnston, S. T., Jeffries, T. E., Pastor-Galán, D., Jenner, G. A., et al. (2011). Iberian late-Variscan granitoids: Some considerations on crustal sources and the significance of "mantle extraction ages". *Lithos* 123 (1-4), 121–132. doi:10.1016/j.lithos.2010.09.010

Ferreira, M., Ferreira, J. T., Puga, E., and Díaz de Federico, A. (1988). Geochronological contribution to the petrogenetic picture of the Betic Chain, SE de España. *Congr. Geol. España* 2, 55–58.

Frizon de Lamotte, D., Saint Bezar, B., Bracène, R., and Mercier, E. (2000). The two main steps of the Atlas building and geodynamics of the Western Mediterranean. *Tectonics* 19 (4), 740–761. doi:10.1029/2000tc900003

Gaina, C., Torsvik, T. H., van Hinsbergen, D. J., Medvedev, S., Werner, S. C., Labails, C., et al. (2013). The african plate: A history of oceanic crust accretion and subduction since the jurassic. *Tectonophysics* 604, 4–25. doi:10.1016/j.tecto.2013.05.037

García-Casco, A., Garcia-Casco, A., and Martin-Algarra, A. (2014). Pre-Alpine discordant granitic dikes in the metamorphic core of the betic cordillera: Tectonic implications. *Terra nova.* 26, 477–486. doi:10.1111/ter.12123

García-Casco, A., and Torres-Roldán, R. L. (1999). Natural metastable reactions involving garnet, staurolite and cordierite: Implications for petrogenetic grids and the extensional collapse of the betic-rif belt. *Contributions Mineralogy Petrology* 136 (1), 131–153. doi:10.1007/s004100050528

García-Dueñas, V., Balanyá, J. C., and Martínez-Martínez, J. M. (1992). Miocene extensional detachments in the outcropping basement of the northern Alboran basin (Betics) and their tectonic implications. *Geo-Marine Lett.* 12 (2), 88–95. doi:10.1007/bf02084917

Gimeno-Vives, O., Mohn, G., Bosse, V., Haissen, F., Zaghloul, M. N., Atouabat, A., et al. (2019). The Mesozoic margin of the Maghrebian Tethys in the Rif belt (Morocco): Evidence for polyphase rifting and related magmatic activity. *Tectonics* 38 (8), 2894–2918. doi:10.1029/2019tc005508

Gómez, J. J., Sandoval, J., Aguado, R., O'Dogherty, L., and Osete, M. L. (2019). "The alpine cycle in eastern Iberia: Microplate units and geodynamic stages," in *The geology of iberia: A geodynamic approach* (New York, US: Springer), 15–27.

Gómez-Pugnaire, M. T., and Franz, G. (1988). Metamorphic evolution of the palaeozoic series of the betic cordilleras (Nevado-Filábride complex, SE Spain) and its relationship with the alpine orogeny. *Geol. Rundsch.* 77 (3), 619–640. doi:10.1007/bf01830174

Gomez-Pugnaire, M. T., Galindo-Zaldívar, J., Rubatto, D., González-Lodeiro, F., Lopez Sanchez-Vizcaino, V., and Jabaloy, A. (2004). A reinterpretation of the nevado-filábride and Alpujárride complexes (betic cordillera): Field, petrography and U-Pb ages from orthogneisses (Western sierra Nevada, S Spain). *Schweiz Min. Petrogr. Mitt* 84 (3), 303–322.

Gómez-Pugnaire, M. T., Nieto, F., Abad, I., Velilla, N., Garrido, C. J., Acosta-Vigil, A., and López Sánchez-Vizcaíno, V. (2019). "Alpine metamorphism in the betic internal zones," in *The geology of iberia: A geodynamic approach* (Cham: Springer), 519–544.

Gómez-Pugnaire, M. T., Rubatto, D., Fernández-Soler, J. M., Jabaloy, A., López-Sánchez-Vizcaíno, V., González-Lodeiro, F., et al. (2012). Late variscan magmatism in the nevado-filábride complex: U-Pb geochronologic evidence for the pre-mesozoic nature of the deepest betic complex (SE Spain). *Lithos* 146, 93–111. doi:10.1016/j.lithos.2012.03.027

Gonzalez-Castillo, L., Galindo-Zaldivar, J., de Lacy, M. C., Borque, M. J., Marínez-Moreno, F. J., García-Armenteros, J. A., et al. (2015). Active rollback in the Gibraltar arc: Evidences from CGPS data in the Western betic cordillera. *Tectonophysics* 663, 310–321. doi:10.1016/j.tecto.2015.03.010

Gretter, N., Ronchi, A., Langone, A., and Perotti, C. R. (2013). The transition between the two major permian tectono-stratigraphic cycles in the central southern Alps: Results from facies analysis and U/Pb geochronology. *Int. J. Earth Sci.* 102 (5), 1181–1202. doi:10.1007/s00531-013-0886-4

Grevemeyer, I., Gràcia, E., Villaseñor, A., Leuchters, W., and Watts, A. B. (2015). Seismicity and active tectonics in the Alboran Sea, Western Mediterranean: Constraints from an offshore-onshore seismological network and swath bathymetry data. *J. Geophys. Res. Solid Earth* 120 (12), 8348–8365. doi:10.1002/2015jb012073

Guerrera, F., Martín-Algarra, A., and Martín-Martín, M. (2012). Tectono-sedimentary evolution of the 'numidian formation'and lateral facies (southern branch of the Western Tethys): Constraints for central-Western mediterranean geodynamics. *Terra nova.* 24 (1), 34–41. doi:10.1111/j.1365-3121.2011.01034.x

Guerrera, F., Martín-Algarra, A., and Perrone, V. (1993). Late oligocene-miocene syn-/-late-orogenic successions in Western and central mediterranean chains from the betic cordillera to the southern apennines. *Terra nova.* 5 (6), 525–544. doi:10.1111/j.1365-3121.1993.tb00302.x

Guerrera, F., Martín-Martín, M., Perrone, V., and Tramontana, M. (2005). Tectono-sedimentary evolution of the southern branch of the western Tethys (maghrebian flysch basin and lucanian ocean): Consequences for western mediterranean geodynamics. *Terra nova..* 17 (4), 358–367. doi:10.1111/j.1365-3121.2005.00621.x

Guerrera, F., Martín-Martín, M., and Tramontana, M. (2021). Evolutionary geological models of the central-Western peri-mediterranean chains: A review. *Int. Geol. Rev.* 63 (1), 65–86. doi:10.1080/00206814.2019.1706056

Gutiérrez-Alonso, G., Fernández-Suárez, J., Jeffries, T. E., Johnston, S. T., Pastor-Galán, D., Murphy, J. B., et al. (2011). Diachronous post-orogenic magmatism within a developing orocline in Iberia, European Variscides. *Tectonics* 30 (5). doi:10.1029/2010tc002845

Handy, M. R., Schmid, S. M., Bousquet, R., Kissling, E., and Bernoulli, D. (2010). Reconciling plate-tectonic reconstructions of Alpine Tethys with the geological–geophysical record of spreading and subduction in the Alps. *Earth-Science Rev.* 102 (3-4), 121–158. doi:10.1016/j.earscirev.2010.06.002

Hebeda, E. H., Boelrijk, N. A. I. M., Priem, H. N. A., Verdurmen, E. T., Verschure, R. H., Simon, O. J., et al. (1980). Excess radiogenic Ar and undisturbed Rb-Sr systems in basic intrusives subjected to Alpine metamorphism in southeastern Spain. *Earth Planet. Sci. Lett.* 47 (1), 81–90. doi:10.1016/0012-821x(80)90106-5

Jabaloy, A., Galindo-Zaldívar, J., and González-Lodeiro, F. (1993). The Alpujárride-Nevado-Fibábride extensional shear zone, Betic Cordillera, SE Spain. *J. Struct. Geol.* 15 (3-5), 555–569. doi:10.1016/0191-8141(93)90148-4

Jabaloy-Sánchez, A., Gómez-Pugnaire, M. T., Padrón-Navarta, J. A., López-Sánchez-Vizcaíno, V. L., and Garrido, C. J. (2015). Subduction-and exhumation-related structures preserved in metaserpentinites and associated metasediments from the Nevado–Filábride Complex (Betic Cordillera, SE Spain). *Tectonophysics* 644, 40–57. doi:10.1016/j.tecto.2014.12.022

Jabaloy-Sánchez, A., Talavera, C., Gómez-Pugnaire, M. T., López-Sánchez-Vizcaíno, V., Vázquez-Vílchez, M., Rodríguez-Peces, M. J., et al. (2018). U-Pb ages of detrital zircons from the internal Betics: A key to deciphering paleogeographic provenance and tectono-stratigraphic evolution. *Lithos* 318, 244–266. doi:10.1016/j.lithos.2018.07.026

Jabaloy-Sánchez, A., Talavera, C., Rodríguez-Peces, M. J., Vázquez-Vílchez, M., and Evans, N. J. (2021). U-Pb geochronology of detrital and igneous zircon grains from the Águilas Arc in the Internal Betics (SE Spain): Implications for Carboniferous-Permian paleogeography of Pangea. *Gondwana Res.* 90, 135–158. doi:10.1016/j.gr.2020.10.013

Jackson, S. E., Pearson, N. J., Griffin, W. L., and Belousova, E. A. (2004). The application of laser ablation-inductively coupled plasma-mass spectrometry to *in situ* U–Pb zircon geochronology. *Chem. Geol.* 211 (1-2), 47–69. doi:10.1016/j.chemgeo.2004.06.017

Kirchner, K. L., Behr, W. M., Loewy, S., and Stockli, D. F. (2016). Early Miocene subduction in the Western Mediterranean: Constraints from Rb-Sr multimineral isochron geochronology. *Geochem. Geophys. Geosyst.* 17 (5), 1842–1860. doi:10.1002/2015gc006208

Kozur, H., Kampschuur, W., Mulder-Blanken, C. W. H., and Simon, O. J. (1974). Contribution to the triassic ostracode faunas of the betic zone (southern Spain). *Scr. Geol.* 23, 1–56.

Laborda-Lopez, C., Aguirre, J., and Donovan, S. K. (2015). Surviving metamorphism: Taphonomy of fossil assemblages in marble and calc-silicate schist. *Palaios* 30 (9), 668–679. doi:10.2110/palo.2015.013

Laborda-López, C., Aguirre, J., Donovan, S. K., Navas-Parejo, P., and Rodríguez, S. (2015). Fossil assemblages and biostratigraphy of metamorphic rocks of the Nevado-Filábride Complex from the Águilas tectonic arc (SE Spain). *Span. J. palaentology* 30 (2), 275–292.

Laborda-López, C., López-Sánchez-Vizcaíno, V., Marchesi, C., Gómez-Pugnaire, M. T., Garrido, C. J., Jabaloy-Sánchez, A., et al. (2018). High-P metamorphism of rodingites during serpentinite dehydration (Cerro del Almirez, Southern Spain): Implications for the redox state in subduction zones. *J. Metamorph. Geol.* 36 (9), 1141–1173. doi:10.1111/jmg.12440

Lafuste, M. L. J., and Pavillon, M. J. (1976). Mise en évidence dEifélien daté au sein des terrains métamorphiques des zones internes des Cordillères bétiques. Intérêt de ce nouveau repére stratigraphique. *Comptes Rendus l'Académie Sci. Paris* 283, 1015–1018.

Lago, M., Gil, A., Arranz, E., Galé, C., and Pocoví, A. (2005). Magmatism in the intracratonic central iberian basins during the permian: Palaeoenvironmental consequences. *Palaeogeogr. Palaeoclimatol. Palaeoecol.* 229 (1-2), 83–103. doi:10.1016/j.palaeo.2005.06.032

Leprêtre, R., Frizon de Lamotte, D., Combier, V., Gimeno-Vives, O., Mohn, G., Eschard, R., et al. (2018). The Tell-Rif orogenic system (Morocco, Algeria, Tunisia) and the structural heritage of the southern Tethys margin. *BSGF - Earth Sci. Bull.* 189 (2), 10. doi:10.1051/bsgf/2018009

Li, B., and Massonne, H. J. (2018). Two tertiary metamorphic events recognized in high-pressure metapelites of the nevado-filábride complex (betic cordillera, S Spain). *J. Metamorph. Geol.* 36 (5), 603–630. doi:10.1111/jmg.12312

Lis Mancilla, F. D., Stich, D., Berrocoso, M., Martín, R., Morales, J., Fernandez-Ros, A., et al. (2013). Delamination in the betic range: Deep structure, seismicity, and GPS motion. *Geology* 41 (3), 307–310. doi:10.1130/g33733.1

Lonergan, L., and Platt, J. P. (1995). The malaguide-alpujárride boundary: A major extensional contact in the internal zone of the eastern betic cordillera, SE Spain. *J. Struct. Geol.* 17 (12), 1655–1671. doi:10.1016/0191-8141(95)00070-t

Lonergan, L., and White, N. (1997). Origin of the Betic-Rif mountain belt. *Tectonics* 16 (3), 504–522. doi:10.1029/96tc03937

López Sánchez-Vizcaíno, V. L., Rubatto, D., Gómez-Pugnaire, M. T., Trommsdorff, V., and Müntener, O. (2001). Middle Miocene high-pressure metamorphism and fast exhumation of the Nevado-Filábride Complex, SE Spain. *Terra nova..* 13 (5), 327–332. doi:10.1046/j.1365-3121.2001.00354.x

López-Gómez, J., Alonso-Azcárate, J., Arche, A., Arribas, J., Fernández Barrenechea, J., Borruel-Abadía, V., and Viseras, C. (2019). "Permian-Triassic rifting stage," in *The geology of iberia: A geodynamic approach* (New York, US: Springer), 29–112.

Manatschal, G., and Müntener, O. (2009). A type sequence across an ancient magma-poor ocean–continent transition: The example of the Western alpine Tethys ophiolites. *Tectonophysics* 473 (1-2), 4–19. doi:10.1016/j.tecto.2008.07.021

Marsh, J. H., and Stockli, D. F. (2015). Zircon U–Pb and trace element zoning characteristics in an anatectic granulite domain: Insights from LASS-ICP-MS depth profiling. *Lithos* 239, 170–185. doi:10.1016/j.lithos.2015.10.017

Martin, J. M., and Braga, J. C. (1987). Alpujárride carbonate deposits (southern Spain)—Marine sedimentation in a triassic atlantic. *Palaeogeogr. Palaeoclimatol. Palaeoecol.* 59, 243–260. doi:10.1016/0031-0182(87)90083-6

Martín-Rojas, I., Somma, R., Delgado, F., Estévez, A., Iannace, A., Perrone, V., et al. (2009). Triassic continental rifting of pangaea: Direct evidence from the Alpujárride carbonates, betic cordillera, SE Spain. *J. Geol. Soc.* 166 (3), 447–458. doi:10.1144/0016-76492008-091

Martín-Rojas, I., Somma, R., Delgado, F., Estévez, A., Iannace, A., Zamparelli, V., et al. (2012). The triassic platform of the gador-turon unit (Alpujárride complex, betic cordillera, southeast Spain): Climate versus tectonic factors controlling platform architecture. *Facies* 58 (2), 297–323. doi:10.1007/s10347-011-0275-z

Martínez-Martínez, J. M., Soto, J. I., and Balanyá, J. C. (2002). Orthogonal folding of extensional detachments: Structure and origin of the sierra Nevada elongated dome (Betics, SE Spain). *Tectonics* 21 (3), 3-1–3-20. doi:10.1029/2001tc001283

Marzoli, A., Callegaro, S., Dal Corso, J., Davies, J. H., Chiaradia, M., Youbi, N., and Jourdan, F. (2018). "The central atlantic magmatic province (CAMP): A review," in *The late triassic world* (New York, US: Springer), 91–125.

McKie, T., and Williams, B. (2009). Triassic palaeogeography and fluvial dispersal across the northwest European Basins. *Geol. J.* 44 (6), 711–741. doi:10.1002/gj.1201

Megard-Galli, J., and Faure, J. L. (1988). Tectonique distensive et sédimentation au Ladinien supérieur-Carnien dans la zone briançonnaise. *Bull. Soc. géologique Fr.* 4 (5), 705–715. doi:10.2113/gssgfbull.iv.5.705

Michard, A., Feinberg, H., El-Azzab, D., Bouybaouene, M., and Saddiqi, O. (1992). A serpentinite ridge in a collisional paleomargin setting: The Beni malek massif, external Rif, Morocco. *Earth Planet. Sci. Lett.* 113 (3), 435–442. doi:10.1016/0012-821x(92)90144-k

Mohn, G., Manatschal, G., Müntener, O., Beltrando, M., and Masini, E. (2010). Unravelling the interaction between tectonic and sedimentary processes during lithospheric thinning in the Alpine Tethys margins. *Int. J. Earth Sci.* 99 (1), 75–101. doi:10.1007/s00531-010-0566-6

Monié, P., Galindo-Zaldívar, J., Lodeiro, F. G., Goffe, B., and Jabaloy, A. (1991). 40Ar/39Ar geochronology of Alpine tectonism in the Betic Cordilleras (southern Spain). *J. Geol. Soc.* 148 (2), 289–297. doi:10.1144/gsjgs.148.2.0289

Montel, J. M. (2000). Preservation of old U-Th-Pb ages in shielded monazite; example from the Beni Bousera Hercynian kinzigites (Morocco). *J. Metamorph. Geol.* 18, 335–342. doi:10.1046/j.1525-1314.2000.00261.x

Morales, J., Molina-Aguilera, A., Mancilla, F., Stich, D., Azañon, J. M., Teixido, T., et al. (2022). Preservation of the Iberian Tethys paleomargin beneath the eastern Betic mountain range. *Gondwana Res.* 106, 237–246. doi:10.1016/j.gr.2022.01.015

Nirrengarten, M., Manatschal, G., Tugend, J., Kusznir, N., and Sauter, D. (2018). Kinematic evolution of the southern North Atlantic: Implications for the formation of hyperextended rift systems. *Tectonics* 37 (1), 89–118. doi:10.1002/2017tc004495

Pastor-Galán, D., Gutiérrez-Alonso, G., Fernández-Suárez, J., Murphy, J. B., and Nieto, F. (2013). Tectonic evolution of NW Iberia during the Paleozoic inferred from the geochemical record of detrital rocks in the Cantabrian Zone. *Lithos* 182, 211–228. doi:10.1016/j.lithos.2013.09.007

Paton, C., Woodhead, J. D., Hellstrom, J. C., Hergt, J. M., Greig, A., Maas, R., et al. (2010). Improved laser ablation U-Pb zircon geochronology through robust downhole fractionation correction. *Geochem. Geophys. Geosyst.* 11 (3). doi:10.1029/2009gc002618

Pedrera, A., Ruiz-Constán, A., García-Senz, J., Azor, A., Marín-Lechado, C., Ayala, C., et al. (2020). Evolution of the South-Iberian paleomargin: From hyperextension to continental subduction. *J. Struct. Geol.* 138, 104122. doi:10.1016/j.jsg.2020.104122

Pereira, M. F., Gama, C., Dias da Silva, Í., Silva, J. B., Hofmann, M., Linnemann, U., et al. (2020). Chronostratigraphic framework and provenance of the ossamorena zone carboniferous basins (southwest Iberia). *Solid earth.* 11 (4), 1291–1312. doi:10.5194/se-11-1291-2020

Pereira, M. F., Ribeiro, C., Vilallonga, F., Chichorro, M., Drost, K., Silva, J. B., et al. (2014). Variability over time in the sources of south Portuguese zone turbidites: Evidence of denudation of different crustal blocks during the assembly of pangaea. *Int. J. Earth Sci.* 103 (5), 1453–1470. doi:10.1007/s00531-013-0902-8

Perri, F., Critelli, S., Martín-Algarra, A., Martín-Martín, M., Perrone, V., Mongelli, G., et al. (2013). Triassic redbeds in the malaguide complex (betic cordillera—Spain): Petrography, geochemistry and geodynamic implications. *Earth-Science Rev.* 117, 1–28. doi:10.1016/j.earscirev.2012.11.002

Perrone, V., Martín-Algarra, A., Critelli, S., Decandia, F. A., D'errico, M., Estevez, A., et al. (2006). 'Verrucano'and 'pseudoverrucano'in the central-western mediterranean alpine chains: Palaeogeographical evolution and geodynamic significance. *Geol. Soc. Lond. Spec. Publ.* 262 (1), 1–43. doi:10.1144/gsl.sp.2006.262.01.01

Petrus, J. A., and Kamber, B. S. (2012). VizualAge: A novel approach to laser ablation ICP-MS U-Pb geochronology data reduction. *Geostand. Geoanalytical Res.* 36 (3), 247–270. doi:10.1111/j.1751-908x.2012.00158.x

Platt, J. P., Anczkiewicz, R., Soto, J. I., Kelley, S. P., and Thirlwall, M. (2006). Early Miocene continental subduction and rapid exhumation in the Western Mediterranean. *Geol.* 34 (11), 981. doi:10.1130/g22801a.1

Platt, J. P., Behr, W. M., Johanesen, K., and Williams, J. R. (2013). The betic-rif arc and its orogenic hinterland: A review. *Annu. Rev. Earth Planet. Sci.* 41, 313–357. doi:10.1146/annurev-earth-050212-123951

Platt, J. P. (2007). From orogenic hinterlands to mediterranean-style back-arc basins: A comparative analysis. *J. Geol. Soc.* 164 (2), 297–311. doi:10.1144/0016-76492006-093

Platt, J. P., Kelley, S. P., Carter, A., and Orozco, M. (2005). Timing of tectonic events in the Alpujárride complex, betic cordillera, southern Spain. *J. Geol. Soc.* 162 (3), 451–462. doi:10.1144/0016-764903-039

Poulaki, E. M., Stockli, D. F., Shuck, B., Laskari, S., and Stockli, L. (2020). Unraveling the pre-subduction stratigraphy and tectonometamorphic evolution of deeply subducted and exhumed rocks using zircon U-Pb geochronology. *AGU Fall Meet. Abstr.* 2020, 0411–V102.

Puga, E., Fanning, C. M., Nieto, J. M., and De Federico, A. D. (2005). Recrystallization textures in zircon generated by ocean-floor and eclogite-facies metamorphism: A cathodoluminescence and U–Pb SHRIMP study, with constraints from REE elements. *Can. Mineralogist* 43 (1), 183–202. doi:10.2113/gscanmin.43.1.183

Puga, E., De Federico, A. D., and Nieto, J. M. (2002). Tectonostratigraphic subdivision and petrological characterisation of the deepest complexes of the betic zone: A review. *Geodin. Acta* 15 (1), 23–43. doi:10.1016/s0985-3111(01)01077-4

Puga, E., Díaz de Federico, A., Fanning, M., Nieto, J. M., Rodríguez Martínez-Conde, J. Á., Díaz Puga, M. Á., et al. (2017). The betic ophiolites and the mesozoic evolution of the western Tethys. *Geosciences* 7 (2), 31. doi:10.3390/geosciences7020031

Puga, E., Fanning, M., de Federico, A. D., Nieto, J. M., Beccaluva, L., Bianchini, G., et al. (2011). Petrology, geochemistry and U–Pb geochronology of the betic ophiolites: Inferences for pangaea break-up and birth of the westernmost Tethys Ocean. *Lithos* 124 (3-4), 255–272. doi:10.1016/j.lithos.2011.01.002

Rehault, J. P., Boillot, G., and Mauffret, A. (1984). The Western Mediterranean basin geological evolution. *Mar. Geol.* 55 (3-4), 447–477. doi:10.1016/0025-3227(84)90081-1

Ribeiro, M. L., Castro, A., Almeida, A., Menéndez, L. G., Jesus, A., Lains, J. A., and Solá, A. R. (2019). "Variscan magmatism," in *The geology of iberia: A geodynamic approach* (New York, US: Springer), 497–526.

Rodríguez-Cañero, R., Jabaloy-Sánchez, A., Navas-Parejo, P., and Martín-Algarra, A. (2018). Linking palaeozoic palaeogeography of the betic cordillera to the variscan iberian massif: New insight through the first conodonts of the nevado-filábride complex. *Int. J. Earth Sci.* 107 (5), 1791–1806. doi:10.1007/s00531-017-1572-8

Romagny, A., Jolivet, L., Menant, A., Bessière, E., Maillard, A., Canva, A., et al. (2020). Detailed tectonic reconstructions of the Western Mediterranean region for the last 35 Ma, insights on driving mechanisms. *BSGF - Earth Sci. Bull.* 191 (1), 37. doi:10.1051/bsgf/2020040

Rosenbaum, G., Lister, G. S., and Duboz, C. (2002). Reconstruction of the tectonic evolution of the Western mediterranean since the oligocene. *J. Virt. Ex.* 8. doi:10.3809/jvirtex.2002.0039

Rossetti, F., Faccenna, C., and Crespo-Blanc, A. (2005). Structural and kinematic constraints to the exhumation of the Alpujárride complex (central betic cordillera, Spain). *J. Struct. Geol.* 27 (2), 199–216. doi:10.1016/j.jsg.2004.10.008

Rossetti, F., Lucci, F., Theye, T., Bouybaouenne, M., Gerdes, A., Opitz, J., et al. (2020). Hercynian anatexis in the envelope of the Beni Bousera peridotites (Alboran Domain, Morocco): Implications for the tectono-metamorphic evolution of the deep crustal roots of the Mediterranean region. *Gondwana Res.* 83, 157–182. doi:10.1016/j.gr.2020.01.020

Rossetti, F., Theye, T., Lucci, F., Bouybaouene, M. L., Dini, A., Gerdes, A., et al. (2010). Timing and modes of granite magmatism in the core of the alboran domain, Rif chain, northern Morocco: Implications for the alpine evolution of the Western mediterranean. *Tectonics* 29 (2). doi:10.1029/2009tc002487

Royden, L., and Faccenna, C. (2018). Subduction orogeny and the late cenozoic evolution of the mediterranean arcs. *Annu. Rev. Earth Planet. Sci.* 46, 261–289. doi:10.1146/annurev-earth-060115-012419

Sainz, A. C., and Faccenna, C. (2001). Tertiary compressional deformation of the Iberian plate. *Terra nova.* 13 (4), 281–288. doi:10.1046/j.1365-3121.2001.00355.x

Sánchez-Navas, A., García-Casco, A., Mazzoli, S., and Martín-Algarra, A. (2017). Polymetamorphism in the Alpujárride complex, betic cordillera, south Spain. *J. Geol.* 125 (6), 637–657. doi:10.1086/693862

Sánchez-NavasGarcía-Casco, A., and Martín-Algarra, A. (2014). *Pre-Alpine discordant granitic dikes in the metamorphic core of the Betic Cordillera: tectonic implications Terra*, 26, 477–486. doi:10.1111/ter.12123*Nova*

Sánchez-Rodríguez, L., and Gebauer, D. (2000). Mesozoic formation of pyroxenites and gabbros in the ronda area (southern Spain), followed by early Miocene subduction metamorphism and emplacement into the middle crust: U–Pb sensitive high-resolution ion microprobe dating of zircon. *Tectonophysics* 316 (1-2), 19–44. doi:10.1016/s0040-1951(99)00256-5

Sánchez-Vizcaíno, V. L., Rubatto, D., Gómez-Pugnaire, M. T., Trommsdorff, V., and Müntener, O. (2001). Middle Miocene high-pressure metamorphism and fast exhumation of the Nevado-Filábride Complex, SE Spain. *Terra nova.* 13 (5), 327–332. doi:10.1046/j.1365-3121.2001.00354.x

Santamaría-López, Á., Lanari, P., and Sanz de Galdeano, C. S. (2019). Deciphering the tectono-metamorphic evolution of the Nevado-Filábride complex (Betic Cordillera, Spain)–A petrochronological study. *Tectonophysics* 767, 128158. doi:10.1016/j.tecto.2019.06.028

Santamaría-López, Á., and Sanz de Galdeano, C. (2018). SHRIMP U–Pb detrital zircon dating to check subdivisions in metamorphic complexes: A case of study in the nevado–filábride complex (betic cordillera, Spain). *Int. J. Earth Sci.* 107 (7), 2539–2552. doi:10.1007/s00531-018-1613-y

Sanz de Galdeano, C., and Santamaría-López, Á. (2019). *The lithological sequence of the Nevado-Filábride complex (Betic internal zone) in the Sierras Nevada and filabres La secuencia litológica del Complejo Nevado-Filábride (Zona Interna Bética) en las sierras Nevada y de los Filabres*. Madrid, Spain: Sociedad Geológica de España.

Sanz de Galdeano, C. S., Garrido, Á. C. L., and Santamaría-López, Á. (2016). Major scale structure of the marbles situated between Cóbdar and Macael (Nevado-Filábride Complex, Betic Cordillera, Almería province, Spain), and general stratigraphic arrangement. *Rev. Soc. Geol. España* 29 (2), 107–116.

Sanz de Galdeano, C. S., López-Garrido, A. C., GarcÍa-Tortosa, F. J., and Delgado, F. (1997). Nuevas observaciones en el Alpujárride del sector centro-Occidental de la sierra de Carrascoy (Murcia). Consecuencias paleogeográficas. *Estud. Geol.* 53 (5-6), 229–236.

Saspiturry, N., Cochelin, B., Razin, P., Leleu, S., Lemirre, B., Bouscary, C., et al. (2019). Tectono-sedimentary evolution of a rift system controlled by Permian post-orogenic extension and metamorphic core complex formation (Bidarray Basin and Ursuya dome, Western Pyrenees). *Tectonophysics* 768, 228180. doi:10.1016/j.tecto.2019.228180

Schettino, A., and Turco, E. (2009). Breakup of Pangaea and plate kinematics of the central Atlantic and Atlas regions. *Geophys. J. Int.* 178 (2), 1078–1097. doi:10.1111/j.1365-246x.2009.04186.x

Schoene, B., and Bowring, S. A. (2006). U–Pb systematics of the McClure mountain syenite: Thermochronological constraints on the age of the 40Ar/39Ar standard MMhb. *Contrib. Mineral. Pet.* 151 (5), 615–630. doi:10.1007/s00410-006-0077-4

Sharman, G. R., Sharman, J. P., and Sylvester, Z. (2018). detritalPy: A Python-based toolset for visualizing and analysing detrital geo-thermochronologic data. *Depos. Rec.* 4 (2), 202–215. doi:10.1002/dep2.45

Sibuet, J. C., Rouzo, S., and Srivastava, S. (2012). Plate tectonic reconstructions and paleogeographic maps of the central and North Atlantic oceans[1]This article is one of a series of papers published in this CJES Special Issue on the theme of*Mesozoic–Cenozoic geology of the Scotian Basin.*[2]Earth Sciences Sector Contribution 20120172. *Can. J. Earth Sci.* 49 (12), 1395–1415. doi:10.1139/e2012-071

Sibuet, J. C., Srivastava, S. P., and Spakman, W. (2004). Pyrenean orogeny and plate kinematics. *J. Geophys. Res.* 109 (B8). doi:10.1029/2003jb002514

Simancas, J. F. (2018). A reappraisal of the alpine structure of the Alpujárride complex in the betic cordillera: Interplay of shortening and extension in the westernmost mediterranean. *J. Struct. Geol.* 115, 231–242. doi:10.1016/j.jsg.2018.08.001

Sláma, J., Košler, J., Condon, D. J., Crowley, J. L., Gerdes, A., Hanchar, J. M., et al. (2008). Plešovice zircon—A new natural reference material for U–Pb and Hf isotopic microanalysis. *Chem. Geol.* 249 (1-2), 1–35. doi:10.1016/j.chemgeo.2007.11.005

Sopeña, A., López, J., Arche, A., Pérez-Arlucea, M., Ramos, A., Virgili, C., et al. (1988). Permian and Triassic rift basins of the iberian peninsula. *Dev. Geotect.* 22, 757–786. doi:10.1016/B978-0-444-42903-2.50036-1

Soto, J. I., Flinch, J. F., and Tari, G. (2017). "Permo-triassic basins and tectonics in Europe, north Africa and the atlantic margins: A synthesis," in *Permo-triassic salt provinces of Europe, north Africa and the atlantic margins* (Amsterdam, Netherlands: Elsevier), 3–41.

Spencer, C. J., Kirkland, C. L., and Taylor, R. J. (2016). Strategies towards statistically robust interpretations of *in situ* U–Pb zircon geochronology. *Geosci. Front.* 7 (4), 581–589. doi:10.1016/j.gsf.2015.11.006

Stampfli, G. M., and Borel, G. D. (2002). A plate tectonic model for the Paleozoic and Mesozoic constrained by dynamic plate boundaries and restored synthetic oceanic isochrons. *Earth Planet. Sci. Lett.* 196 (1-2), 17–33. doi:10.1016/s0012-821x(01)00588-x

Stampfli, G. M., and Kozur, H. W. (2006). Europe from the variscan to the alpine cycles. *Geol. Soc. Lond. Memoirs* 32, 57–82. doi:10.1144/gsl.mem.2006.032.01.04

Stephan, T., Kroner, U. W. E., and Romer, R. L. (2019). The pre-orogenic detrital zircon record of the Peri-Gondwanan crust. *Geol. Mag.* 156 (2), 281–307. doi:10.1017/s0016756818000031

Storck, J. C., Brack, P., Wotzlaw, J. F., and Ulmer, P. (2019). Timing and evolution of middle triassic magmatism in the southern Alps (northern Italy). *J. Geol. Soc.* 176 (2), 253–268. doi:10.1144/jgs2018-123

Talavera, C., Montero, P., Bea, F., González Lodeiro, F., and Whitehouse, M. (2013). U–Pb zircon geochronology of the Cambro-Ordovician metagranites and metavolcanic rocks of central and NW Iberia. *Int. J. Earth Sci.* 102 (1), 1–23. doi:10.1007/s00531-012-0788-x

Tera, F., and Wasserburg, G. J. (1972). U-Th-Pb systematics in three Apollo 14 basalts and the problem of initial Pb in lunar rocks. *Earth Planet. Sci. Lett.* 14 (3), 281–304. doi:10.1016/0012-821x(72)90128-8

Thomson, S. N., Gehrels, G. E., Ruiz, J., and Buchwaldt, R. (2012). Routine low-damage apatite U-Pb dating using laser ablation–multicollector–ICPMS. *Geochem. Geophys. Geosyst.* 13 (2). doi:10.1029/2011gc003928

Tubía, J. M., Cuevas, J., Esteban, J. J., and Gil Ibarguchi, J. I. (2009). Remnants of a Mesozoic rift in a subducted terrane of the Alpujárride complex (betic cordilleras, southern Spain). *J. Geol.* 117 (1), 71–87. doi:10.1086/593322

Tubía, J. M., and Ibarguchi, J. G. (1991). Eclogites of the ojen nappe: A record of subduction in the Alpujárride complex (betic cordilleras, southern Spain). *J. Geol. Soc.* 148 (5), 801–804. doi:10.1144/gsjgs.148.5.0801

Van Hinsbergen, D. J., Torsvik, T. H., Schmid, S. M., Maṭenco, L. C., Maffione, M., Vissers, R. L., et al. (2020). Orogenic architecture of the Mediterranean region and kinematic reconstruction of its tectonic evolution since the Triassic. *Gondwana Res.* 81, 79–229. doi:10.1016/j.gr.2019.07.009

van Hinsbergen, D. J., Vissers, R. L., and Spakman, W. (2014). Origin and consequences of Western Mediterranean subduction, rollback, and slab segmentation. *Tectonics* 33 (4), 393–419. doi:10.1002/2013tc003349

Vergés, J., and Fernàndez, M. (2012). Tethys–atlantic interaction along the iberia–africa plate boundary: The betic–rif orogenic system. *Tectonophysics* 579, 144–172. doi:10.1016/j.tecto.2012.08.032

Vermeesch, P. (2018). IsoplotR: A free and open toolbox for geochronology. *Geosci. Front.* 9 (5), 1479–1493. doi:10.1016/j.gsf.2018.04.001

Vermeesch, P. (2013). Multi-sample comparison of detrital age distributions. *Chem. Geol.* 341, 140–146. doi:10.1016/j.chemgeo.2013.01.010

Villaseca, C., Belousova, E., Orejana, D., Castiñeiras, P., and Pérez-Soba, C. (2011). Presence of Palaeoproterozoic and Archean components in the granulite-facies rocks of central Iberia: The Hf isotopic evidence. *Precambrian Res.* 187 (1-2), 143–154. doi:10.1016/j.precamres.2011.03.001

Vissers, R. L. M., and Meijer, P. T. (2012). Iberian plate kinematics and Alpine collision in the Pyrenees. *Earth-Science Rev.* 114 (1-2), 61–83. doi:10.1016/j.earscirev.2012.05.001

Vissers, R. L. M. (1992). Variscan extension in the pyrenees. *Tectonics* 11 (6), 1369–1384. doi:10.1029/92tc00823

Williams, J. R., and Platt, J. P. (2018). A new structural and kinematic framework for the Alborán Domain (Betic–Rif arc, Western Mediterranean orogenic system). *J. Geol. Soc.* 175 (3), 465–496. doi:10.1144/jgs2017-086

Wissink, G. K., Wilkinson, B. H., and Hoke, G. D. (2018). Pairwise sample comparisons and multidimensional scaling of detrital zircon ages with examples from the North American platform, basin, and passive margin settings. *Lithosphere* 10 (3), 478–491. doi:10.1130/l700.1

Zeck, H. P. (1996). Betic-rif orogeny: Subduction of mesozoic Tethys lithosphere under eastward drifting Iberia, slab detachment shortly before 22 Ma, and subsequent uplift and extensional tectonics. *Tectonophysics* 254 (1-2), 1–16. doi:10.1016/0040-1951(95)00206-5

Zeck, H. P., and Whitehouse, M. J. (1999). Hercynian, Pan-African, Proterozoic and Archean ion-microprobe zircon ages for a Betic-Rif core complex, Alpine belt, W Mediterranean–consequences for its PTt path. *Contrib. Mineral. Pet.* 134 (2), 134–149. doi:10.1007/s004100050474